

MULTIGRID WITH LINEAR STORAGE COMPLEXITY ^{*}

DANIEL BAUER [†], NILS KOHL [‡], STEPHEN F. MCCORMICK [§], AND
RASMUS TAMSTORF [¶]

Abstract. As the discretization error for the solution of a partial differential equation (PDE) decreases, the precision required to store the corresponding coefficients naturally increases. Storing the solution's finite element coefficients explicitly requires $\mathcal{O}(n \log n)$ bits of storage, where n is the number of degrees of freedom (DoFs). This paper presents a full multigrid method to compute the solution in a compressed format that reduces the storage complexity of the solution and intermediate vectors to $\mathcal{O}(n)$ bits. This reduction allows a matrix-free implementation to solve elliptic PDEs with an overall linear space complexity. For problems limited by the memory capacity of current supercomputers, we expect a memory footprint reduction of about an order of magnitude compared to state-of-the-art mixed-precision methods. We demonstrate the applicability of our algorithm by solving two model problems. Depending on the PDE and polynomial degree, but irrespective of the problem size, the solution vector on the finest grid requires between 4 and 12 bits per DoF, and the residual and correction require 3 to 6 bits each. Additional data is stored on the coarse grids with modestly increasing bit widths toward coarser grids.

Key words. compact multigrid, mixed precision, data compression, block-floating point

MSC codes. 65G50, 65N22, 65N55, 65Y04, 65Y20

1. Introduction. Discretization of a partial differential equation (PDE) generally induces a *discretization error* that limits the accuracy of the computed solution. These errors occur of course in any such setting because a solution in an infinite-dimensional space cannot be expected to be exactly represented by a finite-dimensional computation. In the following, our focus is on a fully regular elliptic PDE of order $2m$ discretized by the finite element method (FEM) on a uniform grid of mesh size h using polynomials of degree p . In this setting, the energy norm of the discretization error is of order h^{p-m+1} [25].

In practice, the finite element approximation of the solution is stored as a vector of coefficients, each quantized to finite precision with unit roundoff ε . This introduces a second kind of error, the *quantization error* [26]. The discrete energy norm of this error is $\mathcal{O}(\kappa^{1/2}\varepsilon)$, where κ is the condition number of the discretized linear operator A [20]. Because $\kappa \in \mathcal{O}(h^{-2m})$ grows as the grid is refined [25], so does the quantization error if ε is kept fixed. Thus, for small enough h , the quantization error dominates the discretization error, leading to poor accuracy; cf. Figure 1.

An efficient PDE solver must aim to balance both sources of error. It would be a waste of computational resources to reduce one significantly, while letting the other

^{*}The author/s would like to thank the NHR-Verein e.V. (www.nhr-verein.de) for supporting this work/project within the NHR Graduate School of National High Performance Computing (NHR). The authors gratefully acknowledge support through the joint project CoMPS (<https://gauss-allianz.de/en/project/title/CoMPS>) (grant 16ME0647K) funded by the German Federal Ministry of Research, Technology and Space. The authors gratefully acknowledge the Gauss Centre for Supercomputing e.V. (<https://www.gauss-centre.eu>) for funding this project by providing computing time on the GCS Supercomputer SuperMUC-NG and friendly user access during the pilot operation of the GCS Supercomputer SuperMUC-NG Phase 2 at Leibniz Supercomputing Centre (<https://www.lrz.de>).

[†]Friedrich-Alexander-Universität Erlangen-Nürnberg (FAU), Erlangen National High Performance Computing Center (NHR@FAU), (daniel.j.bauer@fau.de).

[‡]Dept. of Earth and Environmental Sciences, Ludwig-Maximilians-Universität München (LMU).

[§]University of Colorado at Boulder, Boulder, CO.

[¶]Independent researcher.

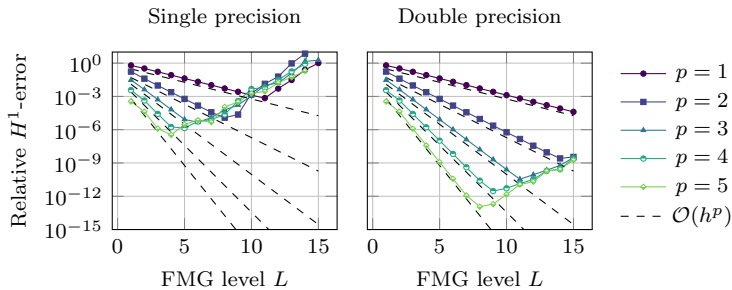


FIG. 1. Solving the homogeneous Poisson equation on the unit interval for the manufactured solution $u(x) = x(1-x) \cos(\frac{\pi}{2}x)$. The problem is discretized with B-spline finite elements of degree p and solved by a “textbook” full multigrid solver executed in an a priori fixed floating point precision. The error ceases to decrease with the expected rate of $\mathcal{O}(h^p)$ as the limit of the finite precision is reached. A higher precision allows for finer grids, but any fixed bit-width constrains the attainable accuracy.

severely limit the accuracy of the solution. Therefore, the precision ε must be of order h^{p+1} , assuming that the above bounds are sharp. Given ε , the number of bits used to represent each coefficient of the solution is $\mathcal{O}(\log \varepsilon^{-1})$. For a regular grid, the grid spacing h is related to the number of degrees of freedom (DoFs) n in that $h \approx n^{-1/d}$, where d is the dimension of the domain. So it follows that the number of bits per coefficient must increase with $\log n$, implying that the solution vector requires $\mathcal{O}(n \log n)$ bits of storage. We emphasize that this result is about quantizing the exact solution vector and is independent of how the solution is found.

In this work, we develop a full multigrid (FMG) solver to compute the solution in a compressed format, reducing the storage complexity to $\mathcal{O}(n)$ bits while maintaining discretization-error-accuracy. In addition to the solution vector, the precisions of matrices and other vectors appearing in FMG must also increase as the grid is refined [20, 26]. We show how our algorithm can be implemented with linear storage complexity overall. Among other things, this is achieved by operating matrix-free.

The basic idea behind the compression is to leverage the smoothness that the solution to an elliptic PDE exhibits by virtue of the natural assumptions about the source term and sufficient regularity. Due to smoothness, the solution at two neighboring locations cannot differ by more than some bounded amount, and the closer the two locations are to each other, the tighter this bound becomes. Loosely speaking, the difference between two DoFs that are spatially close together must be in their trailing bits, while the information contained in the leading bits is largely redundant.

To avoid this redundancy, the multigrid hierarchy can be used to compress the solution. Initially restricting the discussion to just two grids, instead of discretizing the solution on the fine grid directly, it can be split into a coarse approximation (stored on the coarse grid) and a fine correction (stored on the fine grid). At first this may seem counter-productive, given that it requires additionally storing the coarse-grid approximation. However, storing an approximation on the coarse grid is comparatively cheap, and, critically, the smoothness of the solution ensures that the magnitude of the fine-grid correction is small, meaning that it can be stored in reduced precision. Generalizing to a multigrid hierarchy, the solution can be disassembled into a coarsest-grid approximation and successive corrections on the finer grids. Due to smoothness, the corrections get progressively smaller in magnitude toward increasingly finer grids, and thus can be stored in low precision without losing accuracy.

This idea goes back to [22], where it was termed *compact multigrid data structure*. However, algorithms to compute the solution in compact form were presented under the assumption that the system matrix and right-hand side (RHS) can be stored in fixed precision, which is not generally sufficient to achieve discretization-error accuracy [20, 26]. Moreover, [22] does not address how to compute the residual with linear space complexity, despite this computation being the most sensitive to rounding error [20, 26]. The same compression idea as in [22] has been realized in [27] using hierarchical bases on sparse grids. However, the presented solver relies on the system matrix being diagonal, essentially eliminating its practical value.

Compressing the output of numerical simulations has also been studied decoupled from the numerical method underlying the simulation; see [17] for an overview. While this cannot reduce the memory cost of the simulation, the motivation is to reduce the size of the output on permanent storage and/or make post-processing feasible [17]. The authors of [1, 18] draw on the ideas of a multigrid hierarchy, and separate the input data into different scales by a series of matrix-vector products and linear system solves. The scales are stored on a multigrid hierarchy and then further compressed through level-dependent quantization and using an external compression algorithm. In [23, 15], wavelets are used to achieve a similar decomposition. Because the input data of these methods need not be further specified, they are independent of the numerical solver and offer great flexibility. However, with no connection to the underlying problem/theory, it is unclear what an acceptable bound for the compression error may be. Our approach integrates the compression with the FMG solver, enabling us to select quantization precisions in such a way that even the compressed data is as accurate as the discretization allows.

In this work, we adopt the compact representation idea of [22] to develop algorithms to solve elliptic PDEs to discretization-error accuracy, with linear bit-complexity in space. To the authors' knowledge, it is the first general implementation of a PDE solver that can attain discretization-error accurate solutions with $\mathcal{O}(n)$ storage. For state-of-the-art problems limited by memory capacity [10], we expect a memory footprint reduction of about an order of magnitude.

The rest of the paper is structured as follows. [Section 2](#) describes the compact format and [section 3](#) introduces the compact multigrid algorithm. In subsequent sections, we discuss the algorithm's precision requirements ([section 4](#)), optimize its memory consumption to linear bit-complexity ([section 5](#)), and study the associated cost ([section 6](#)). Finally, [section 7](#) presents numerical experiments and [section 8](#) summarizes our conclusions.

2. Compact representation. To formally introduce the compact representation, we first establish some notation. The objective is to find the solution $u(x)$ of an elliptic PDE, $\mathcal{L}u(x) = f(x)$, with $u(x)$ in the solution space V of functions of x in the domain Ω . To solve the PDE, we discretize it on a set of $L + 1$ nested grids corresponding to finite-dimensional subspaces, $V_0 \subset \dots \subset V_L \subset V$. Each of these n_ℓ -dimensional subspaces, V_ℓ for $0 \leq \ell \leq L$, is spanned by a set of finite element basis functions. We can collect these basis functions in a (covariant) row vector $\Phi_\ell(x)$, having n_ℓ elements, each element being a basis function. Because the spaces V_ℓ are nested, there are prolongation matrices $P_\ell \in \mathbb{R}^{n_\ell \times n_{\ell-1}}$ from level $\ell - 1$ to level ℓ such that

$$(1) \quad \Phi_{\ell-1}(x) = \Phi_\ell(x)P_\ell.$$

Using the FEM basis, the approximate solution on level ℓ , denoted $u_\ell(x)$, can be

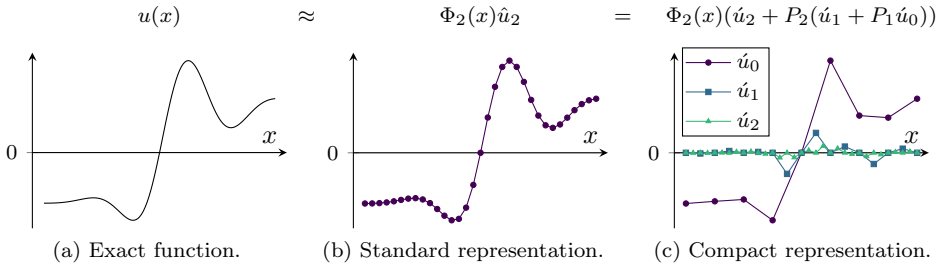


FIG. 2. An example function discretized with piecewise-linear elements. The basis on level 2 is denoted by the row vector $\Phi_2(x)$. In standard representation, only the finest grid is used. In contrast, the compact vector consists of a coarse approximation and two successively finer corrections. Crucially, the magnitude of the corrections decreases toward increasingly finer grids, allowing them to be stored in lower precision without significant loss of accuracy.

written as

$$(2) \quad u_\ell(x) = \Phi_\ell(x) \hat{u}_\ell \in V_\ell,$$

where $\hat{u}_\ell \in \mathbb{R}^{n_\ell}$ is the (contravariant) column vector of FEM coefficients. We also call \hat{u}_ℓ the *standard representation* of $u_\ell(x)$.

The *compact representation* of the function $u_L(x)$ is a set of $L+1$ sections $\acute{u}_\ell \in \mathbb{R}^{n_\ell}$ for each level ℓ , $0 \leq \ell \leq L$, which fulfills

$$(3) \quad \hat{u}_L = \acute{u}_L + P_L(\acute{u}_{L-1} + P_{L-1}(\cdots + P_1 \acute{u}_0)).$$

To refer to the collection of all compact sections on grids 0 to L , we write $\acute{u}_{0:L}$, or \acute{u} for brevity. To emphasize, we distinguish the function $u_L(x) \in V_L$, its FEM coefficient vector $\hat{u}_L \in \mathbb{R}^{n_L}$ decorated with a hat, and the coefficient vectors of the compact sections $\acute{u}_{0:L} \in \bigotimes_{\ell=0}^L \mathbb{R}^{n_\ell}$ marked with an acute accent. A sketch of a function and its standard and compact representations is given in [Figure 2](#).

2.1. Precision requirements. If the hierarchy comprises at least two levels, there are infinitely many compact representations $\acute{u}_{0:L}$ fulfilling (3) due to the nested nature of the spaces V_ℓ [12]. Given one compact vector, any function can be added to grid ℓ if it is also subtracted from the next finer grid $\ell + 1$ to construct a different representation of the same function. Even a degenerate compact representation is possible where only the finest section is nonzero. Thus, how many bits are required to store each section cannot be answered universally. In this latter example, the finest section has to equal the standard representation while all other sections are zero. Hence, this particular compact representation has the same storage cost as the standard representation: the precision of the finest section increases with the number of levels [20, 26] while the coarse sections require zero bits.

Storage savings are obtained by compact representations whose coarse sections closely approximate the continuous function. Consider the special example of a fully regular second-order elliptic PDE. If the RHS is in $L^2(\Omega)$, then the solution is in $H^2(\Omega)$ [25] and the best finite element approximations in the *energy norm* (defined in the lemma) converge to the solution in the $H^1(\Omega)$ norm. The following lemma shows that the segment of the best energy approximation on a fine grid, defined as the difference between the best fine- and coarse-grid energy approximations, vanishes in the energy norm sense as $L \rightarrow \infty$.

LEMMA 1. Consider a second-order PDE, written in weak form as

$$(4) \quad \text{Find } u \in H^1(\Omega) \text{ such that } a(u, v) = b(v) \quad \forall v \in H^1(\Omega),$$

where $a(u, v)$ is a symmetric $H^1(\Omega)$ bounded and coercive bilinear form and $b(v)$ is a linear form, both derived from weakening the strong form $\mathcal{L}u = f$ of the PDE. Consider the energy norm $a(\cdot, \cdot)^{1/2}$. As $L \rightarrow \infty$, the difference between the best energy approximations to u from V_L and V_{L-1} vanishes in the energy norm sense.

Proof. The first result here about energy orthogonality between the best energy approximation $u_L \in V_L$ to the PDE solution $u \in H^1(\Omega)$ and its error $t := u - u_L$ is a well-known basic principle in some contexts. See [25], for example. Note that the energy orthogonality of $u_L \in V_L$ and t follows naturally from the property that u_L is the energy-orthogonal projection of u onto V_L . Nevertheless, the proof is included here for completeness and because an analogous argument leads to the discrete case that the same holds for the best energy approximation $u_{L-1} \in V_{L-1}$ to u_L . This discrete result then provides the basis for establishing the lemma.

The best energy approximation $u_L \in V_L$ to $u \in H^1(\Omega)$ is, by definition,

$$(5) \quad u_L = \operatorname{argmin}_{v_L \in V_L} a(v_L - u, v_L - u).$$

To establish the energy orthogonality that we need, note first that

$$(6) \quad \begin{aligned} a(v_L - u, v_L - u) &= a(v_L - u_L, v_L - u_L) + 2a(v_L - u_L, u_L - u) + a(u_L - u, u_L - u) \\ &= a(v_L - u_L, v_L - u_L) + C, \end{aligned}$$

where $C = a(u_L - u, u_L - u)$ is a constant w.r.t. v_L . The assertion here is that the term $a(v_L - u_L, u_L - u)$ vanishes because $u_L - u$ is energy-orthogonal to V_L . Were it not, then we could determine a nonzero $\delta_L \in V_L$ so that $u_L - u + \delta_L$ is energy-orthogonal to V_L , but that leads to the following contradiction to (5) for any $s \in (0, \frac{2}{3})$:

$$\begin{aligned} a(u_L + s\delta_L - u, u_L + s\delta_L - u) &= a(u_L - u, u_L - u) + 2sa(\delta_L, u_L + s\delta_L - u) + s^2a(\delta_L, \delta_L) \\ &= a(u_L - u, u_L - u) + 2sa(\delta_L, u_L - u + \delta_L + (s-1)\delta_L) + s^2a(\delta_L, \delta_L) \\ &= a(u_L - u, u_L - u) + 2sa(\delta_L, (s-1)\delta_L) + s^2a(\delta_L, \delta_L) \\ &= a(u_L - u, u_L - u) + (3s-2)sa(\delta_L, \delta_L) \\ &< a(u_L - u, u_L - u)! \end{aligned}$$

Note now by energy orthogonality of t and V_L that

$$\begin{aligned} a(v_{L-1} - u, v_{L-1} - u) &= a(v_{L-1} - u_L + t, v_{L-1} - u_L + t) \\ &= a(v_{L-1} - u_L, v_{L-1} - u_L) + a(t, t). \end{aligned}$$

Since $a(t, t)$ is independent of v_{L-1} , then this expansion shows that the best energy approximation u_{L-1} to u from V_{L-1} is the arg min of $a(v_{L-1} - u_L, v_{L-1} - u_L)$ over $v_{L-1} \in V_{L-1}$. An argument analogous to that above then shows that the error $t_L = u_L - u_{L-1}$ is energy-orthogonal to V_{L-1} .

All of this development goes to show that $u_L = u_{L-1} + t_L$ is an energy-orthogonal decomposition, which means of course that the only difference between u_{L-1} and u_L is the segment t_L . The energy norm of t_L must therefore vanish as $L \rightarrow \infty$ because u_L converges in energy to u , thus proving the lemma. \square

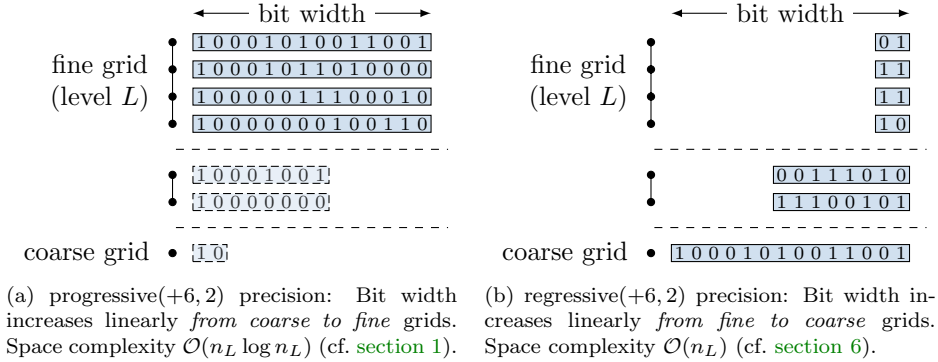


FIG. 3. Sketch of a vector in standard representation (progressive precision) and compact representation (regressive precision). The level index increases from bottom to top, and bits become less significant from left to right. In the compact case, all sections $u_{0:L}$ are stored as a whole, while in standard representation the finest grid vector represents the entire solution. The bit width of the finest compact section is independent of L while the precisions of all coarser sections increase with L . The shown bit-values are made up and serve only illustrative purposes.

By Lemma 1, the segments t_L of the energy-orthogonal decomposition vanish in energy as $L \rightarrow \infty$. This in turn implies that the bits representing t_L must be zero (relative to the full representation of u_L) up to a small number of trailing bits. This justifies the assumption in this work of the existence of a compact representation that can be stored in *regressive precision*, by which we mean that

$$(7) \quad k(L - \ell) + b$$

bits are used to store the compact section on level ℓ , where k and b are constants independent of L and ℓ . That is, the precision of the finest section (b bits) is independent of the number of levels L , and the number of bits used for the coarser sections increases (by k bits) toward increasingly coarser grids. We will denote regressive precision as *regressive(+ k , b)*, where the plus sign serves as a reminder that the first argument is the increment. Section 6 details why the total number of bits is linear in this case. The term “regressive” is chosen in analogy to *progressive* precision from [20, 26], where the precision increases with the refinement level: If a hierarchy of vectors is stored in *progressive(+ k , b)* precision, b bits are used on the coarsest grid, and this precision increases by k bits for each level of refinement.

To achieve discretization-error accuracy, the standard representation of the solution of the PDE requires *progressive(+ $p + 1$, b)* precision [20, 26]. Below we demonstrate experimentally that the solution’s compact representation can be stored in regressive precision, using the same increment of $p + 1$ bits. In essence, the precision hierarchy is flipped, so that now the fine-grid vectors—comprising most DoFs of the multigrid hierarchy—are stored in fixed and low precision, instead of requiring an ever-increasing number of bits per DoF. Figure 3 illustrates both ways of storing the solution.

2.2. Compact vector operations. According to (3), the FEM coefficient vector \hat{u}_L can be recovered by summing all compact sections after prolongating them to the finest grid. Converting a compact representation vector to standard representation in this way is straightforward and requires only $\mathcal{O}(n_L)$ operations. The reverse

conversion is more involved. For example, the decomposition of [1] requires obtaining L^2 projections onto the coarse grids, which involves solving a variational problem, and in multiresolution analysis the decomposition matrices are generally not sparse unless biorthogonal wavelets are constructed [24]. We will not go into details here and instead show how to compute the solution from the PDE directly in compact form, eliminating the need for a compactification routine.

Multiplying a compact vector with a scalar α is as simple as multiplying each section with α . Likewise, sums and general linear combinations of compact vectors can be formed on each section individually because they commute with the prolongations in (3). It is worth noting that the scalar α in the multiplication $\hat{y}_{0:L} \leftarrow \alpha_{0:L} \hat{x}_{0:L}$ can vary with the level. We exploited this successfully to implement an additive Bramble-Pasciak-Xu (BPX)-like [4] multigrid method by varying the smoothing rate depending on the level. However, adequate rates are problem-specific and non-trivial to find, so we focus instead on multiplicative multigrid in this paper.

Prolongating a compact vector amounts to introducing a zero-valued correction on the new fine-grid. If the vector is stored in regressive($+k, b$) precision, the precision of the new finest section is b bits. Because the number of levels L increases in (7), the precision of all other sections is adjusted by k bits.

3. Compact multigrid. In this section, we discuss how the FMG algorithm can be adapted so that it computes the solution in compact format. Our goals are to keep the excellent convergence properties of FMG, i.e., linear complexity w.r.t. the number of arithmetic operations, and to compute a compact solution that can be stored in regressive precision, i.e., with linear space complexity. This section focuses on the storage cost of the solution, and is not concerned with reducing the memory footprint of other quantities. In a second step, we optimize the remaining parts of the algorithm in section 5.

We base our algorithm on the full approximation scheme (FAS) variant of multigrid, briefly defined below. For details, the reader is referred to [5, 6]. For convenience, the supplement distills the relevant ideas into this article’s notation. FAS owes its name to computing a full approximation to the fine-grid solution on each grid of the hierarchy. Precisely this property is helpful to compute a compact solution, so we choose FAS over the for linear problems equivalent and more “standard” correction scheme (CS).

3.1. Full approximation scheme. The objective is to solve an elliptic PDE discretized on refinement level L as $A_L \hat{y}_L = \hat{r}_L$. We further define standard multigrid components [5, 6]:

- the prolongation matrices $P_\ell \in \mathbb{R}^{n_\ell \times n_{\ell-1}}$, $1 \leq \ell \leq L$, that canonically arise from the nesting of the FEM spaces as outlined in the previous section,
- the restriction matrices $R_\ell \in \mathbb{R}^{n_{\ell-1} \times n_\ell}$, $1 \leq \ell \leq L$, that transfer vectors from one grid to the next coarser grid and are typically defined as $R_\ell := P_\ell^T$,
- coarse-grid operators $A_\ell := R_{\ell+1} A_{\ell+1} P_{\ell+1}$, $0 \leq \ell < L$, arising through Galerkin coarsening,
- and, for all ℓ , $0 \leq \ell \leq L$, a smoother of the form [7, 2]

$$(8) \quad \hat{y}_\ell \leftarrow \hat{y}_\ell + M_\ell(\hat{r}_\ell - A_\ell \hat{y}_\ell).$$

Both CS and FAS use the smoother to reduce oscillatory errors and obtain an approximate solution \hat{y}_L . While CS uses the next coarser grid to find a smooth correction \hat{d}_{L-1} , the FAS coarse-grid variable approximates the full solution to the

fine-grid equation. It is defined as

$$(9) \quad \hat{y}_{L-1} := \tilde{R}_L \hat{y}_L + \hat{d}_{L-1},$$

where \tilde{R}_L is a restriction operator defined on the finite-element solution space V_L , unlike R_L which is defined on the dual space of V_L . (Technically, the matrices \tilde{R}_L and R_L restrict the vector representations of elements of V_L and its dual.) One typically has some freedom in choosing \tilde{R} without sacrificing efficiency [5]. We comment on our choice in [subsection 3.2](#).

In FAS, \hat{y}_{L-1} is found by (approximately) solving the coarse-grid equation

$$(10) \quad A_{L-1} \hat{y}_{L-1} = R_L \hat{r}_L + \underbrace{(A_{L-1} \tilde{R}_L \hat{y}_L - R_L A_L \hat{y}_L)}_{\hat{\tau}_L},$$

where $\hat{\tau}_L$ is known as the *fine-to-coarse defect correction*. It modifies the coarse-grid equation so that at convergence its solution coincides with the (restricted) fine-grid solution $\tilde{R}_L A_L^{-1} \hat{r}_L$.

After having found a good approximation on the coarse grid through recursion, the fine-grid variable is updated according to

$$(11) \quad \hat{y}_L \leftarrow \hat{y}_L + P_L \hat{d}_{L-1} = \hat{y}_L + P_L (\hat{y}_{L-1} - \tilde{R}_L \hat{y}_L).$$

3.2. Compact full approximation scheme. Now we adapt FAS to compute a compact solution $\hat{y}_L = \acute{y}_L + P_L (\acute{y}_{L-1} + P_{L-1} (\dots + P_1 \acute{y}_0))$. Inserting the compact representation into the fine-grid equation gives

$$(12) \quad A_L (\acute{y}_L + P_L (\acute{y}_{L-1} + P_{L-1} (\dots + P_1 \acute{y}_0))) = \hat{r}_L.$$

Before applying a smoother to (12), the equation must be reformulated w.r.t. a single solution variable. To that end, note that the smoother primarily affects oscillatory components and, hence, its main effect should be on the finest compact section. This motivates moving the coarse sections to the RHS, giving an equation for just the finest section:

$$(13) \quad A_L \acute{y}_L = \hat{r}_L - \underbrace{A_L (P_L (\acute{y}_{L-1} + P_{L-1} (\dots + P_1 \acute{y}_0)))}_{\hat{v}_L}.$$

If a smoother of the form (8) is used, then smoothing on (13) is equivalent to smoothing on the original fine-grid equation. It is important that the pre-smoother has little effect on smooth components, as is commonly the case. Solving (13) exactly instead of “just” applying a smoother would introduce modes from the full spectrum into \acute{y}_L . However, only if modes of different frequency, which are of different magnitude in general, are separated, can $\acute{y}_{0:L}$ be stored in regressive precision. For the post-smoother, this is less relevant, because at the time it is applied, the smooth modes have already been solved for and stored in the coarse sections $\acute{y}_{0:L-1}$.

After the smoothing step, we turn our attention to solving the FAS coarse-grid equation (10). This requires defining the primal-space restriction operator \tilde{R} . Because this operator is only applied to the compact vector $\acute{y}_{0:L}$, the canonical choice is to drop the finest section:

$$(14) \quad \tilde{R}_L (\acute{y}_L + P_L (\acute{y}_{L-1} + P_{L-1} (\dots + P_1 \acute{y}_0))) := \acute{y}_{L-1} + P_{L-1} (\dots + P_1 \acute{y}_0).$$

With this implicit definition at hand (and using the Galerkin condition $A_{L-1} = R_L A_L P_L$), the defect correction from (10) simplifies to $\hat{\tau}_L = -R_L A_L \acute{y}_L$. Remarkably, $\hat{\tau}_L$ depends only on the finest section \acute{y}_L instead of on the entire vector \hat{y}_L as in (10). Again, moving all coarser sections to the RHS gives an equation for the section \acute{y}_{L-1} :

$$(15) \quad A_{L-1} \acute{y}_{L-1} = R_L \hat{\tau}_L - \underbrace{R_L A_L \acute{y}_L}_{-\hat{\tau}_L} - \underbrace{A_{L-1} (P_{L-1} \acute{y}_{L-2} + \cdots + P_{L-1} \cdots P_1 \acute{y}_0)}_{\hat{v}_{L-1}}.$$

Like the fine-grid equation (13), the coarse-grid equation (15) is solved by applying a smoother and solving a coarse-grid equation. To display the pattern, we give the equation on the next coarser grid, which involves another $\hat{\tau}$ -term but otherwise looks familiar:

$$(16) \quad A_{L-2} \acute{y}_{L-2} = R_{L-1} R_L \hat{\tau}_L - R_{L-1} \underbrace{R_L A_L \acute{y}_L}_{-\hat{\tau}_L} - \underbrace{R_{L-1} A_{L-1} \acute{y}_{L-1}}_{-\hat{\tau}_{L-1}} - \hat{v}_{L-2}.$$

This process is repeated until a coarse enough grid is reached, where solving the equation is trivial.

To summarize, compact FAS improves the approximation $\acute{y}_{0:L}$ by relaxing for all levels $\ell = 0, \dots, L$ on the equation

$$(17) \quad \begin{aligned} A_\ell \acute{y}_\ell &= \hat{\tau}_\ell - \hat{s}_\ell - \hat{v}_\ell, \\ \hat{\tau}_\ell &:= R_{\ell+1} \cdots R_L \hat{\tau}_L, \\ \hat{s}_\ell &:= -(\hat{\tau}_{\ell+1} + \cdots + \hat{\tau}_L) = R_{\ell+1} (A_{\ell+1} \acute{y}_{\ell+1} + R_{\ell+2} (\cdots + A_L \acute{y}_L)), \\ \hat{v}_\ell &:= A_\ell \hat{z}_\ell, \\ \hat{z}_\ell &:= P_\ell (\acute{y}_{\ell-1} + P_{\ell-1} (\cdots + P_1 \acute{y}_0)). \end{aligned}$$

The order in which the levels are handled can be chosen freely to determine the cycle structure. For example, a V(1,0)-cycle handles the finest level first and the coarsest level last, while a V(0,1)-cycle works from the coarsest toward the finest grid. Unlike in a standard CS or FAS cycle, no coarse-grid corrections are applied, because smooth and oscillatory components are separated in the compact representation.

Algorithm 1 lists the steps of the compact V(0,1) FAS scheme though the algorithm can be easily modified to include more pre-/post-smoothing steps. Later, in section 4, we discuss how much precision is needed for the various quantities appearing in the algorithm. While these results should not concern us yet, different precisions are represented by different colors and change of precision is denoted by underlines.

Algorithm 1 starts with a sweep from finest to coarsest grid, computing \hat{s} on all grids (lines 1 to 3). Importantly, the recursive structure of \hat{s} is exploited to keep the number of floating point operations (flops) linear. The fine-to-coarse sweep is followed by a coarse-to-fine sweep that computes the prolonged standard representation $\hat{z}_\ell := P_\ell (\acute{y}_{\ell-1} + P_{\ell-1} (\cdots + P_1 \acute{y}_0))$ (lines 4 and 7) and applies the smoother to (17) (lines 5 and 8) on every grid. Again, we benefit from the recursive structure of \hat{z} , which allows us to maintain a linear number of flops.

Algorithm 1 cFAS: Compact V(0,1) full approximation scheme.

| | | | |
|---------------|-----------------|---------------------------|--|
| | $A_{0:L}$ | matrix hierarchy | |
| | $M_{0:L}$ | smoother | |
| <i>Input.</i> | $P_{1:L}$ | prolongation matrices | |
| | $R_{1:L}$ | restriction matrices | |
| | $\hat{y}_{0:L}$ | initial guess of solution | |
| | $\hat{r}_{0:L}$ | RHS | |

Output. Solution $\hat{y}_{0:L}$ improved by one V(0,1) multigrid cycle.

| | | | |
|---|--|---|--|
| | \triangleright <i>Fine-to-coarse sweep.</i> | } | <i>If the initial guess is zero ($\hat{y} = 0$), \hat{s} is zero, requires no storage, and the fine-to-coarse sweep can be left out. In subsection 3.4, we wrap this algorithm in iterative refinement so that the initial guess is indeed zero.</i> |
| 1 | $\hat{s}_L \leftarrow 0$ | | |
| 2 | for $\ell = (L - 1) \dots 0$ step -1 | | |
| 3 | $\hat{s}_\ell \leftarrow R_{\ell+1} A_{\ell+1} \hat{y}_{\ell+1} \nabla + R_{\ell+1} \hat{s}_{\ell+1}$ | | |
| | \triangleright <i>Coarse-to-fine sweep.</i> | | |
| 4 | $\hat{z}_0 \leftarrow 0$ | | |
| 5 | $\hat{y}_0 \leftarrow \hat{y}_0 \blacklozenge + M_0 (\hat{r}_0 \blacklozenge - \hat{s}_0 \blacklozenge - A_0 \hat{y}_0 \blacklozenge) \blacktriangle$ | | \triangleright Smooth $A_0 \hat{y}_0 = \hat{r}_0 - \hat{s}_0$ |
| 6 | for $\ell = 1 \dots L$ step 1 | | |
| 7 | $\hat{z}_\ell \leftarrow P_\ell \hat{y}_{\ell-1} \blacklozenge + P_\ell \hat{z}_{\ell-1} \blacklozenge \nabla$ | | |
| 8 | $\hat{y}_\ell \leftarrow \hat{y}_\ell \blacklozenge + M_\ell (\hat{r}_\ell \blacklozenge - \hat{s}_\ell \blacklozenge - A_\ell \hat{z}_\ell \blacklozenge - A_\ell \hat{y}_\ell \blacklozenge) \blacktriangle$ | | \triangleright Smooth $A_\ell \hat{y}_\ell = \hat{r}_\ell - \hat{s}_\ell - A_\ell \hat{z}_\ell$ |
| 9 | return $\hat{y}_{0:L}$ | | |

Another way to present the compact FAS equations (17) is as a block-system

$$(18) \quad \mathcal{A}_L \begin{pmatrix} \hat{y}_L \\ \hat{y}_{L-1} \\ \vdots \\ \hat{y}_0 \end{pmatrix} = \begin{pmatrix} \hat{r}_L \\ R_L \hat{r}_L \\ \vdots \\ R_1 \cdots R_L \hat{r}_L \end{pmatrix},$$

$$\mathcal{A}_L := \begin{pmatrix} A_L & A_L P_L & \cdots & A_L P_L \cdots P_1 \\ R_L A_L & A_{L-1} & \cdots & A_{L-1} P_{L-1} \cdots P_1 \\ \vdots & \vdots & \ddots & \vdots \\ R_1 \cdots R_L A_L & R_1 \cdots R_{L-1} A_{L-1} & \cdots & A_0 \end{pmatrix}.$$

Here, the terms \hat{s} and \hat{v} have been moved to the left-hand side leading to all the off-diagonal blocks. Multiplication of the block-lower-triangular part of \mathcal{A}_L and \hat{y} gives \hat{s} , and by multiplying the block-upper-triangular part with \hat{y} , we get \hat{v} .

Remarkably, a Gauss-Seidel iteration on (18) is equivalent to a V-cycle with one Gauss-Seidel pre-smoothing step [12]. Similarly, when using Gauss-Seidel in [Algorithm 1](#), it is equivalent to Gauss-Seidel on (18), when the blocks are handled in reverse order. [Equation \(18\)](#) has previously been derived in [12] by discretizing the linear operator from the full set of basis functions from all levels. There, it is noted that this system is semi-definite, and various multilevel methods can be implemented by an iterative method on the block-system. For example, an additive V-cycle can be implemented by applying block-Jacobi [12].

3.3. Residual computation. Although [Algorithm 1](#) can be used as a stand-alone solver, it must be embedded in an FMG scheme to be sure to achieve discretization-error accuracy with linear work. Moreover, we want to benefit from the analysis of [20, 26] and wrap the V-cycle into an iterative refinement (IR) loop. Thus, we need a way to determine the residual $\hat{r} = \hat{f} - A\hat{u}$, where \hat{u} is an approximate solution to the equation $A\hat{u} = \hat{f}$. The difficulty is that only the compact representation \hat{u} is available.

Algorithm 2 FMGRESIDUAL: FMG residual computation.

| | | |
|---------------|-----------------|------------------------|
| | A_L | matrix |
| | $P_{1:L}$ | prolongation matrices |
| <i>Input.</i> | $R_{1:L}$ | restriction matrices |
| | \hat{f}_L | RHS |
| | $\hat{u}_{0:L}$ | solution approximation |

Output. Residual $\hat{r}_\ell = R_{\ell+1} \cdots R_L(\hat{f}_L - A_L(\hat{u}_L + \cdots + P_L \cdots P_1 \hat{u}_0))$ for $0 \leq \ell \leq L$.

▷ Decode solution.

- 1 $\hat{u}_0 \leftarrow \hat{u}_0$
- 2 **for** $\ell = 1 \dots L$ **step** 1
- 3 | $\hat{u}_\ell \leftarrow \hat{u}_\ell + \frac{P_\ell}{\Delta} \hat{u}_{\ell-1}$

▷ Compute residual.

- 4 $\hat{t}_L \leftarrow \hat{f}_L - \frac{A_L}{\Delta} \hat{u}_L$
- 5 $\hat{r}_L \leftarrow \hat{t}_{L_\Delta}$

▷ Restrict residual.

- 6 **for** $\ell = (L-1) \dots 0$ **step** -1
- 7 | $\hat{t}_\ell \leftarrow \frac{R_{\ell+1}}{\Delta} \hat{t}_{\ell+1}$
- 8 | $\hat{r}_\ell \leftarrow \hat{t}_{\ell_\Delta}$
- 9 **return** $\hat{r}_{0:L}$

Our proposed algorithm (Algorithm 2) to compute the residual from the compact solution $\hat{u}_{0:L}$ is straightforward: First, the standard representation \hat{u}_L corresponding to $\hat{u}_{0:L}$ is computed in a sweep from coarsest to finest grid by evaluating (3) (lines 1 to 3). Next, the actual residual computation follows on line 4. After the computation, the result can be truncated to a potentially lower precision (line 5). Finally, a fine-to-coarse sweep through the grid hierarchy determines the restriction of the residual on all coarser grids (lines 6 to 8). This is done so that the hierarchy of residuals $\hat{r}_{0:L}$ can serve as input to the V-cycle Algorithm 1. We remark that the structure of Algorithm 2 resembles an up-side-down V-cycle.

Because the precision required to store the standard representation \hat{u}_ℓ grows with the level ℓ [20], implementing Algorithm 2 with linear space complexity requires some care. This issue is discussed in section 5.

3.4. Compact full multigrid. Finally, we have all the pieces to present the compact FMG solver for the equation $\mathcal{L}u(x) = f(x)$ in Algorithm 3. In lines 1 and 5, the linear operator \mathcal{L} and RHS $f(x)$ are discretized on level L before forming the matrix hierarchy by Galerkin coarsening. The coarse-grid solver in line 2 is exactly the same as in a standard method—on the coarsest grid, the standard and compact representation coincide.

Every time a new FMG level is reached, the current solution approximation is prolonged to this level in line 4. Because it is represented compactly, this amounts to adding a new zero-initialized grid; no matrix-vector products need to be evaluated. Remember from (7) that the number of bits of a regressive-precision quantity on level ℓ depends on the total number of levels L . Therefore, incrementing L and adding a new grid also involves increasing the precision of all other levels, so that regressive precision is maintained throughout the hierarchy.

Next, the residual is computed (line 7) and subsequently used to solve—using a few V-cycles—for the correction (lines 8 to 10). Finally, the correction is applied to the solution in line 11 by adding each section of the compact correction to the solution. Residual computation and correction are repeated for a sufficient number

Algorithm 3 cFMG: Compact FMG.

| | | |
|--------------------------|---|--|
| \mathcal{L} | continuous linear operator | |
| $f(x)$ | continuous RHS | |
| <i>Input.</i> L_{\max} | index of finest grid | |
| N | number of IR iterations per FMG level | |
| ν | number of V-cycles per IR iteration | |
| <i>Output.</i> | Compact solution $\hat{u}_{0:L_{\max}}$. | |

| | | |
|----|--|---|
| 1 | $(A_0, \hat{f}_0) \leftarrow \text{DISCRETIZE}(\mathcal{L}, f(x), L = 0)$ | |
| 2 | $\hat{u}_0 \leftarrow A_0^{-1} \hat{f}_0$ | \triangleright Coarse grid solve. |
| 3 | for $L = 1 \dots L_{\max}$ step 1 | |
| 4 | $\hat{u}_L \leftarrow 0$ | \triangleright Prolongate $\hat{u}_{0:L-1}$. |
| 5 | $(A_{0:L}, M_{0:L}, P_{1:L}, R_{1:L}, \hat{f}_L) \leftarrow \text{DISCRETIZE}(\mathcal{L}, f(x), L)$ | |
| 6 | repeat N times | |
| 7 | $\hat{r}_{0:L} \leftarrow \text{FMGRESIDUAL}(A_L, P_{1:L}, R_{1:L}, \hat{f}_L, \hat{u}_{0:L})$ | \triangleright Algorithm 2. |
| 8 | $\hat{y}_{0:L} \leftarrow 0$ | |
| 9 | repeat ν times | |
| 10 | $\hat{y}_{0:L} \leftarrow \text{CFAS}(A_{0:L_{\nabla}}, M_{0:L_{\nabla}}, P_{1:L_{\nabla}}, R_{1:L_{\nabla}}, \hat{y}_{0:L}, \hat{r}_{0:L})$ | \triangleright V-cycle, Algorithm 1. |
| 11 | $\hat{u}_{0:L} \leftarrow \hat{u}_{0:L} + \hat{y}_{0:L}$ | \triangleright Apply correction. |
| 12 | return $\hat{u}_{0:L_{\max}}$ | |

of IR iterations N .

4. Precision and rounding. While the algorithms presented in the previous section can be used “as is”, the sole motivation for formulating them is to put strict limits on the precision of vectors, with the goal of reducing the total memory footprint to $\mathcal{O}(n)$ bits. Therefore, we now focus our attention on which precision is required for vector and matrix entries in the above algorithms. Some of these precisions are founded in the theory of [20, 26], while everything not covered by existing theory is based on experimental evidence. To ensure that as many results from [20, 26] can be carried over, in the remaining parts of the paper, we restrict the number of V-cycles per IR iteration to one, i.e., we set $\nu = 1$ in Algorithm 3. A convenient consequence is that the initial guess $\hat{y}_{0:L}$ in the V-cycle Algorithm 1 is zero. Thus, the initial fine-to-coarse sweep need not be computed, and $\hat{s}_\ell = 0$ for all ℓ and need not be stored. Hence, we do not specify a precision for \hat{s} . However, we remark that in practice it might be more efficient to increase the number of V-cycles per IR iteration to reduce the number of residual calculations, even though it may come at the cost of requiring slightly higher precision in the inner solver.

The precisions that we have determined are listed in Table 1. The values of b_1, \dots, b_4 are problem-specific and are discussed in section 7. We require that the matrices A , P , and R and RHS \hat{f} are free of any error besides that stemming from quantization. For example, if quadrature is used to evaluate integrals, the resulting error must be insignificant compared to quantization. Regressive and progressive precisions change over the course of the FMG-cycle (w.r.t. L) and during each V-cycle (w.r.t. ℓ), cf. (7).

To aid the reader, quantities in Algorithms 1 to 3 are colored according to their precision listed in Table 1. Frequently, quantities stored in different precisions are used together in an operation, e.g., a vector addition. To make it clear which precision the arithmetic is performed in and what the precision of the result is, we explicitly adapt the precision of (one of) the input argument(s) so that both operands share the same precision. We implement decreasing the precision as rounding toward the nearest representation in the lower precision, breaking ties to even, and increasing the

TABLE 1

Precisions used for vectors and matrix entries. L is the current FMG level. The constants b_1, \dots, b_4 depend on the smoothness of the solution and RHS. We experimentally determine suitable constants for some example problems in [section 7](#).

| Quantity | Precision | Symbol |
|------------------------------------|----------------------------------|--------|
| \hat{u} | regressive(+ $p + 1, b_1$) | ▲ |
| \hat{r}, \hat{y} | regressive(+ m, b_2) | △ |
| matrices, \hat{f} in FMGRESIDUAL | progressive(+ $p + m + 1, b_3$) | ▼ |
| matrices, \hat{z} in CFAS | progressive(+ m, b_4) | ▽ |
| \hat{u}, \hat{t} in FMGRESIDUAL | $(p + 1)L + b_1$ bits | ● |

precision as extending the binary representation by additional zero bits. To keep the linear algebra in the pseudocodes comprehensible, we denote change of precision by an underline and a symbol. The symbol for each precision is listed in [Table 1](#). Once the operands have been converted, the operation is performed within this precision, subject to the usual floating point (FP) rounding behavior. In case of matrix vector products / stencil applications, this entails several rounding steps internally. For example, $A_\ell \underline{\hat{u}}_{\ell_\Delta}$ indicates that the precision of the vector is adapted before evaluating the product in the precision of the matrix. By contrast, in $\underline{A}_\ell \hat{u}_{\ell_\Delta}$, matrix and vector already share the same precision and the result is converted after computing the matrix-vector product.

As discussed previously, the solution \hat{u} is stored in regressive precision. It uses the same precision increment as dictated by existing theory [\[20, 26\]](#), but crucially the increment is now toward coarser grids. The constant b_1 , i.e., the number of bits used on level L , depends on the PDE, the discretization, etc. Likewise, the correction and residual can be stored in regressive precision. As before, we adopt the same increment as used in [\[20, 26\]](#), which is m bits. We do not claim that this is the optimal choice for all PDEs. Since the representation of matrices and RHS remains unchanged compared to previous methods, we cannot expect any storage improvements. Hence, we use the same precision as in [\[20, 26\]](#). Finally, the temporary vectors \hat{z} , \hat{u} , and \hat{t} correspond to the correction in the V-cycle of [\[26\]](#), the standard representation of the solution, and the residual in the FMG-cycle of [\[26\]](#), respectively. Therefore, they use the same respective precisions as in [\[26\]](#). For \hat{u} and \hat{t} , this is the number of bits used for the solution's coarsest compact section. Note that this precision is progressive in L but does not depend on the level index ℓ in [Algorithm 2](#).

In both algorithms, progressive precision matrices are multiplied with vectors that do not use progressive precision. On the coarse grids, the number of bits in the vector is much higher than in the matrix, whereas on the fine grids, the matrix uses more bits. To ensure sufficient accuracy of matrix-vector products, we extend the precision of the arguments before performing the operation (arithmetic and intermediate results). Concretely, we take the precision of the respective matrix on the given level or the precision of the vector's coarsest section (\hat{y}_0 in [Algorithm 1](#), \hat{u}_0 in [Algorithm 2](#)), whichever is higher. In either case, the precision is denoted by red font and conversion to that precision by \blacklozenge . The number of bits depends on ℓ and L , and is different in both algorithms. We do not claim that this choice is necessarily optimal.

5. Memory optimization. As shown in [Table 1](#), the solution, residual, and correction can be stored in regressive precision with linear storage cost. However, the matrices A , P , and R , the RHS, and some temporary vectors require progressive precision, and thus have superlinear storage cost. This section addresses how

Algorithms 1 and 2 can be implemented instead with $\mathcal{O}(n)$ memory.

5.1. Matrices and RHS. The storage cost of matrices becomes irrelevant if the method is implemented matrix-free. Whenever memory footprint is a concern, a matrix-free implementation should be considered before thinking about reducing the storage cost of vectors (the scope of this work), as matrices typically require significantly more memory than vectors. Moreover, matrix-free methods have been shown to outperform matrix-based approaches due to the typical imbalance of memory bandwidth and compute performance of modern hardware [16].

Likewise, an analytically given RHS can be assembled on-the-fly so that it requires practically no memory. If the RHS data is not known analytically but instead stored on disk, it can be read in streaming fashion, without ever loading it completely to memory. In case the RHS arises from the solution of a different PDE and overall linear space complexity is desired, the RHS must be computed and stored in compact format as well. A compact RHS can be decoded in the coarse-to-fine sweep of the residual calculation (Algorithm 2) exactly like the solution. All mentioned approaches lead to linear memory footprint.

5.2. Temporary vectors. The key idea behind matrix-free methods is to never store the entire matrix but only a few select values that are required to determine the result of the operator application at the current DoF/element. Similarly, we limit the memory consumption of the temporary vectors $\hat{z}_{0:L}$, $\hat{u}_{0:L}$, and $\hat{t}_{0:L}$ by minimizing the number of entries that are simultaneously present in memory.

Consider the coarse-to-fine sweep of Algorithm 1 as an example. It iterates over the grid hierarchy computing $\hat{z}_{0:L}$ and from it $\hat{y}_{0:L}$. Crucially, for all levels ℓ , \hat{z}_ℓ is needed only temporarily, to compute \hat{y}_ℓ and $\hat{z}_{\ell+1}$. As soon as these dependent quantities have been derived, \hat{z}_ℓ can be evicted from memory. The time each individual entry of \hat{z}_ℓ must reside in memory, and thus the total number of values stored at the same time, can be minimized by traversing the grid hierarchy in a specific order.

To find this ordering, we exploit the locality of stencil applications, i.e., the sparsity pattern of the matrices. Due to locality, the computation of \hat{y}_ℓ and $\hat{z}_{\ell+1}$ can begin before all entries of \hat{z}_ℓ have been computed. The key strategy is to compute dependent values as soon as possible with the available data in \hat{z}_ℓ . This loosely corresponds to a depth-first search (DFS) traversal of the dependency graph, while the naive variant is closely related to breadth-first search (BFS). Also due to locality, a certain DoF in \hat{z}_ℓ only influences a few values in the dependent vectors. Hence, this DoF can be evicted from memory as soon as all resulting values have been derived from it. Consequently, only a small portion of \hat{z}_ℓ must reside in memory at a given time.

As a result of the above, $\hat{z}_{0:L}$ and $\hat{y}_{0:L}$ are computed in a local region on *all* grids, instead of on the entire domain on one specific level. Owing to the locality of stencil applications, this requires only data from a small neighborhood. Moreover, only the boundary of the already handled area need be reused in future iterations and must therefore be stored. Because the boundary has codimension one, it covers only $\mathcal{O}(n_\ell^{(d-1)/d})$ points.

More precisely, the number of points that must be stored to compute a matrix-vector product $M\hat{x}$, $M \in \mathbb{R}^{m \times n}$, depends on the matrix' sparsity pattern. Denote by $\text{minColIdx}(M, \rho)$ and $\text{maxColIdx}(M, \rho)$ the minimum and maximum column index of the non-zero entries in row ρ , respectively. To apply the stencil of M at grid point ρ , only DoFs of \hat{x} with indices between $\text{minColIdx}(M, \rho)$ and $\text{maxColIdx}(M, \rho)$ are required. To avoid recomputing DoFs required in future iterations at grid points $\sigma > \rho$, only DoFs with indices smaller than $\min_{\rho \leq \sigma \leq m} \text{minColIdx}(M, \sigma)$ are evicted

Algorithm 4 Intermediate steps for transforming the naive coarse-to-fine sweep (lines 4 to 8) of Algorithm 1 to the optimized version in Algorithm 5.

(a) First, the loop (line 6 in Algorithm 1) is transformed to an equivalent recursive form (highlighted lines).

```

1  $\hat{z}_0 \leftarrow 0$ 
2  $\hat{y}_0 \leftarrow \hat{y}_0 + M_0(\hat{r}_0 - \hat{s}_0 - A_0\hat{y}_0)$ 
3 if  $L > 0$ 
4 |  $(\hat{z}, \hat{y})_{1:L} \leftarrow \text{C2F}(\hat{z}_0, \hat{y}_{0:L}, 1)$ 

```

```

C2F( $\hat{z}_{\ell-1}, \hat{y}_{\ell-1:L}, \ell$ )
5  $\hat{z}_\ell \leftarrow P_\ell \hat{y}_{\ell-1} + P_\ell \hat{z}_{\ell-1}$ 
6  $\hat{y}_\ell \leftarrow \hat{y}_\ell + M_\ell(\hat{r}_\ell - \hat{s}_\ell - A_\ell \hat{z}_\ell - A_\ell \hat{y}_\ell)$ 
7 if  $\ell < L$ 
8 |  $(\hat{z}, \hat{y})_{\ell+1:L} \leftarrow \text{C2F}(\hat{z}_\ell, \hat{y}_{\ell:L}, \ell + 1)$ 
9 return  $(\hat{z}, \hat{y})_{\ell:L}$ 

```

(b) Next, the vector operations (lines 5 and 6 in Algorithm 4a) are written as loops over the grid wherein a stencil application is performed at each node.

```

1  $\hat{z}_0 \leftarrow 0$ 
2  $\hat{y}_0 \leftarrow \hat{y}_0 + M_0(\hat{r}_0 - \hat{s}_0 - A_0\hat{y}_0)$ 
3  $i_0, j_0 \leftarrow n_0$ 
4  $i_{1:L}, j_{1:L} \leftarrow 0_{1:L}$ 
5 if  $L > 0$ 
6 |  $(\hat{z}, i, \hat{y}, j)_{1:L} \leftarrow \text{C2F}(\hat{z}_0, i_{1:L}, \hat{y}_{0:L}, j_{1:L}, 1)$ 

```

```

C2F( $\hat{z}_{\ell-1}, i_{\ell:L}, \hat{y}_{\ell-1:L}, j_{\ell:L}, \ell$ )
7 while  $i_\ell < n_\ell$ 
8 |  $\hat{z}_{\ell, i_\ell} \leftarrow (P_\ell \hat{y}_{\ell-1})_{i_\ell} + (P_\ell \hat{z}_{\ell-1})_{i_\ell}$ 
9 |  $i_\ell \leftarrow i_\ell + 1$ 
10 while  $j_\ell < n_\ell$ 
11 |  $\hat{y}_{\ell, j_\ell} \leftarrow (\hat{y}_\ell + M_\ell(\hat{r}_\ell - \hat{s}_\ell - A_\ell \hat{z}_\ell - A_\ell \hat{y}_\ell))_{j_\ell}$ 
12 |  $j_\ell \leftarrow j_\ell + 1$ 
13 if  $\ell < L$ 
14 |  $(\hat{z}, i, \hat{y}, j)_{\ell+1:L} \leftarrow \text{C2F}(\hat{z}_\ell, i_{\ell+1:L}, \hat{y}_{\ell:L}, j_{\ell+1:L}, \ell + 1)$ 
15 return  $(\hat{z}, i, \hat{y}, j)_{\ell:L}$ 

```

from memory. Therefore, at most

$$(19) \quad \delta(M \in \mathbb{R}^{m \times n}) := \max_{1 \leq \rho \leq m} (\max \text{ColIdx}(M, \rho) - \min_{\rho \leq \sigma \leq m} \min \text{ColIdx}(M, \sigma) + 1)$$

entries of the vector \hat{x} must be stored at a time. Clearly, δ depends on the ordering of the unknowns. On structured grids with lexicographic ordering,

$$(20) \quad \delta(M_\ell) \approx (w(M_\ell) - 1)n_\ell^{\frac{d-1}{d}},$$

where $w(M_\ell)$ is the stencil width of M_ℓ , e.g., 3 for a 3-point stencil in 1D, a 5-point stencil in 2D, or a 7-point stencil in 3D. We show in subsection 6.1.2 that the δ in (20) is sufficiently small to guarantee linear space complexity. In any case, a clever ordering of unknowns can be used to minimize δ . For example, orderings based on space-filling curves come to mind. However, one has to be careful since these typically do not minimize for the *maximum* distance of neighboring nodes, which (19) is based on. In that case, it would be best to limit the cache to values that will actually be reused, instead of storing everything with an index greater or equal to the smallest reused index. Alternatively, a trade-off between buffer size and number of recomputations can be made.

We now apply the above discussion and derive the memory-optimal implementation of the coarse-to-fine sweep in Algorithm 1 through a series of code transformations. First, the iterative sweep can be equivalently written recursively as in Algorithm 4a. For any level index ℓ , $0 < \ell \leq L$, the recursive C2F routine (lines 5 to 9) computes and returns $\hat{z}_{\ell:L}$ and $\hat{y}_{\ell:L}$. Level ℓ is handled directly, and the recursion fills in the finer grids. Analogous to the loop in line 6 of Algorithm 1, the index ℓ is incremented each recursive invocation until the base case $\ell = L$ is reached.

The next transformation is to write the vector operations in lines 5 and 6 of Algorithm 4a as explicit loops over the grid (Algorithm 4b, lines 7 to 12). To that end, arrays of indices $i_{0:L}$ and $j_{0:L}$ are introduced (lines 3 and 4). The index i_ℓ , with

Algorithm 5 cFAs: **Algorithm 1** optimized for linear space complexity.

| | | |
|---------------|------------------------------------|---------------------------|
| | $A_{0:L}$ | matrix hierarchy |
| | $M_{0:L}$ | smoother |
| <i>Input.</i> | $P_{1:L}$ | prolongation matrices |
| | $\hat{y}_{0:L} = \mathbf{0}_{0:L}$ | initial guess of solution |
| | $\hat{r}_{0:L}$ | RHS |

Output. Solution $\hat{y}_{0:L}$ improved by one V(0,1) multigrid cycle.

(a) Main algorithm.

- ▷ *Fine-to-coarse sweep is omitted because $\hat{y}_{0:L} = \mathbf{0}_{0:L}$.*
- ▷ *Coarse-to-fine sweep.*

```

1  $\hat{z}_0 \leftarrow \mathbf{0}$ 
2  $\hat{y}_0 \leftarrow \hat{y}_0 + \underline{M_0}(\hat{r}_0 - \underline{A_0}\hat{y}_0)$  ▷ Smooth  $A_0\hat{y}_0 = \hat{r}_0$ 
3  $i_0, j_0 \leftarrow n_0$  ▷ i: index of next node in  $\hat{z}$ .
4  $i_{1:L}, j_{1:L} \leftarrow \mathbf{0}_{1:L}$  ▷ j: index of next node in  $\hat{v}$ .
5 for  $\ell = 1..(L-1)$  step 1
6 |  $\hat{z}_\ell \leftarrow$  Empty buffer with a capacity of  $\max\{\delta(A_\ell), \delta(P_{\ell+1}), \delta(A_{\ell+1}P_{\ell+1})\}$  DoFs.
7 |  $\hat{z}_L \leftarrow$  Empty buffer with a capacity of  $\delta(A_L)$  DoFs.
8 if  $L > 0$ 
9 |  $(\hat{z}, i, \hat{y}, j)_{1:L} \leftarrow \text{c2F}((\hat{z}, i, \hat{y}, j)_{0:L}, 1)$ 
10 return  $\hat{y}_{0:L}$ 

```

(b) $\text{c2F}((\hat{z}, i, \hat{y}, j)_{\ell-1:L}, \ell)$: Recursive coarse-to-fine sweep.

```

11 while  $i_\ell < n_\ell$  and  $\max\text{ColIdx}(P_\ell, i_\ell) < j_{\ell-1}$  and  $\max\text{ColIdx}(P_\ell, i_\ell) < i_{\ell-1}$  ▷ For all nodes  $i_\ell$ 
    ▷ where  $\hat{z}_\ell$  can be computed.
12 | if capacity of  $\hat{z}_\ell$  is exhausted drop oldest value of  $\hat{z}_\ell$  ▷ Limit memory consumption.
13 |  $\hat{z}_{\ell, i_\ell} \leftarrow \underline{(P_\ell \hat{y}_{\ell-1})}_{i_\ell} + \underline{(P_\ell \hat{z}_{\ell-1})}_{i_\ell}$ 
14 |  $i_\ell \leftarrow i_\ell + 1$ 
15 | while  $j_\ell < n_\ell$  and  $\max\text{ColIdx}(A_\ell, j_\ell) < i_\ell$  ▷ For all nodes  $j_\ell$  where  $\hat{y}_\ell$  can be computed.
16 |  $\hat{y}_{\ell, j_\ell} \leftarrow \underline{(\hat{y}_\ell)}_{j_\ell} + \underline{M_\ell(\hat{r}_\ell - \underline{A_\ell}\hat{z}_\ell - \underline{A_\ell}\hat{y}_\ell)}_{j_\ell}$  ▷ Smooth  $A_\ell\hat{y}_\ell = \hat{r}_\ell - A_\ell\hat{z}_\ell$ 
17 |  $j_\ell \leftarrow j_\ell + 1$ 
18 | if  $\ell < L$ 
    ▷ Process all nodes on finer grids that can be computed with the available data.
19 |  $(\hat{z}, i, \hat{y}, j)_{\ell+1:L} \leftarrow \text{c2F}((\hat{z}, i, \hat{y}, j)_{\ell:L}, \ell + 1)$ 
20 return  $(\hat{z}, i, \hat{y}, j)_{\ell:L}$ 

```

$0 \leq i_\ell \leq n_\ell$, points to the next DoF in \hat{z}_ℓ that must be computed. Likewise, j_ℓ counts the progress of the computation of \hat{y}_ℓ . Through the loops in [lines 7 to 12](#), the respective stencil is applied at each node and the index incremented accordingly. We denote the stencil application of, e.g., P_ℓ to $\hat{y}_{\ell-1}$ at node i_ℓ as $(P_\ell \hat{y}_{\ell-1})_{i_\ell}$.

The crucial step allowing for the memory-optimization is to move the computation of \hat{y}_ℓ and the recursive call ([lines 10 to 14](#) of [Algorithm 4b](#)) into the i_ℓ -loop, as shown in the optimized version [Algorithm 5](#), [lines 15 to 19](#). This way, as soon as a DoF of \hat{z}_ℓ is calculated ([line 13](#) of [Algorithm 5](#)), the computation directly proceeds with the dependent values of \hat{y}_ℓ and the finer grids. Only then does the iteration continue with the next node of \hat{z}_ℓ . Because only certain entries of the dependent vectors can be computed, we introduce additional bound checks in [lines 11](#) and [15](#) of [Algorithm 5](#). Finally, this change in the order in which the nodes are processed allows [line 12](#) to evict DoFs of \hat{z}_ℓ quickly from memory. Therefore, in [lines 5](#) to [7](#), we initialize buffers for $\hat{z}_{1:L}$ with the minimally possible capacity such that the stencils of A and P can be applied at each grid point. As noted above, we assume that the initial guess for \hat{y} is zero, so that $\hat{s} = \mathbf{0}$ and no work has to be done in the fine-to-coarse sweep of [Algorithm 5](#).

[Algorithm 2](#) is optimized in a very similar fashion. The optimized version is

Algorithm 6 FMGRESIDUAL: Algorithm 2 optimized for linear space complexity.

A_L matrix
 $P_{1:L}$ prolongation matrices
Input. $R_{1:L}$ restriction matrices
 \hat{f}_L RHS
 $\hat{u}_{0:L}$ solution approximation
Output. Residual $\hat{r}_\ell = R_{\ell+1} \cdots R_L(\hat{f}_L - A_L(\hat{u}_L + \cdots + P_L \cdots P_1 \hat{u}_0))$ for $0 \leq \ell \leq L$.

(a) Main algorithm.

```

1   $\hat{u}_0 \leftarrow \hat{u}_0$ 
2   $i_0 \leftarrow n_0$   $\triangleright i$ : index of next node in  $\hat{u}$ .
3   $i_{1:L} \leftarrow 0_{1:L}$ 
4   $j_{0:L} \leftarrow 0_{0:L}$   $\triangleright j$ : index of next node in  $\hat{t}$ .
5  for  $\ell = 1..(L-1)$  step 1
6  |  $\hat{u}_\ell \leftarrow$  Empty buffer with a capacity of  $\delta(P_{\ell+1})$  DoFs.
7  |  $\hat{u}_L \leftarrow$  Empty buffer with a capacity of  $\delta(A_L)$  DoFs.
8  |  $\hat{t}_0 \leftarrow$  Empty buffer with a capacity of 1 DoF.
9  for  $\ell = 1..L$  step 1
10 |  $\hat{t}_\ell \leftarrow$  Empty buffer with a capacity of  $\delta(R_\ell)$  DoFs.
11 if  $L > 0$ 
12 |  $(\hat{u}, i)_{1:L}, (\hat{t}, j, \hat{r})_{0:L} \leftarrow \text{C2F}(\hat{u}_{1:L}, (\hat{u}, i)_{0:L}, (\hat{t}, j, \hat{r})_{0:L}, 1)$ 
13 return  $\hat{r}_{0:L}$ 
  
```

(b) C2F($\hat{u}_{\ell:L}, (\hat{u}, i)_{\ell-1:L}, (\hat{t}, j, \hat{r})_{0:L}, \ell$): Recursive coarse-to-fine sweep.

```

13 while  $i_\ell < n_\ell$  and  $\max\text{ColIdx}(P_\ell, i_\ell) < i_{\ell-1}$   $\triangleright$  For all nodes  $i_\ell$  where  $\hat{u}_\ell$  can be computed.
14 | if capacity of  $\hat{u}_\ell$  is exhausted drop oldest value of  $\hat{u}_\ell$   $\triangleright$  Limit memory consumption.
15 |  $\hat{u}_{\ell, i_\ell} \leftarrow \hat{u}_{\ell, i_\ell} + \frac{(P_\ell \hat{u}_{\ell-1})_{i_\ell}}{\bullet}$ 
16 |  $i_\ell \leftarrow i_\ell + 1$ 
17 if  $\ell = L$ 
18 |  $(\hat{t}, j, \hat{r})_{0:L} \leftarrow \text{F2C}((\hat{t}, j, \hat{r})_{0:L}, L)$ 
19 else
20 |  $\triangleright$  Process all nodes on finer grids that can be computed with the available data.
21 |  $(\hat{u}, i)_{\ell+1:L}, (\hat{t}, j, \hat{r})_{0:L} \leftarrow \text{C2F}(\hat{u}_{\ell+1:L}, (\hat{u}, i)_{\ell:L}, (\hat{t}, j, \hat{r})_{0:L}, \ell + 1)$ 
22 return  $(\hat{u}, i)_{\ell:L}, (\hat{t}, j, \hat{r})_{0:L}$ 
  
```

(c) F2C($(\hat{t}, j, \hat{r})_{0:\ell+1}, \ell$): Recursive fine-to-coarse sweep.

```

22  $\text{canApplyStencil} \leftarrow \begin{cases} \max\text{ColIdx}(A_L, j_L) < i_L & \text{if } \ell = L \\ \max\text{ColIdx}(R_{\ell+1}, j_\ell) < j_{\ell+1} & \text{else} \end{cases}$ 
23 while  $j_\ell < n_\ell$  and  $\text{canApplyStencil}$ 
24 | if capacity of  $\hat{t}_\ell$  is exhausted drop oldest value of  $\hat{t}_\ell$ 
25 |  $\hat{t}_{\ell, j_\ell} \leftarrow \begin{cases} \frac{\hat{f}_{L, j_L} - (A_L \hat{u}_L)_{j_L}}{\bullet} & \text{if } \ell = L \\ \frac{(R_{\ell+1} \hat{t}_{\ell+1})_{j_\ell}}{\bullet} & \text{else} \end{cases}$ 
26 |  $\hat{r}_{\ell, j_\ell} \leftarrow \hat{t}_{\ell, j_\ell} \Delta$ 
27 |  $j_\ell \leftarrow j_\ell + 1$ 
28 if  $\ell > 0$ 
29 |  $(\hat{t}, j, \hat{r})_{0:\ell-1} \leftarrow \text{F2C}((\hat{t}, j, \hat{r})_{0:\ell}, \ell - 1)$ 
30 return  $(\hat{t}, j, \hat{r})_{0:\ell}$ 
  
```

displayed in Algorithm 6. The key difference to Algorithm 1 is that the coarse-to-fine sweep is followed by a fine-to-coarse sweep. This manifests in the optimized implementation (Algorithm 6) in that the fine-to-coarse sweep is nested in the coarse-to-fine sweep. Apart from that, the pattern remains the same. Note that we presented recursive forms of the optimized algorithms for ease of derivation, but they have equivalent iterative versions.

6. Cost analysis. In this section, we discuss the cost associated with the above algorithms. Storage, computation, and memory transfers are considered.

6.1. Storage. We predicate that the implementation is matrix-free so that the cost to store stencils/matrices and the RHS can be ignored. Below, we show that mantissas and exponents of all vectors can be stored with $\mathcal{O}(n_L)$ bits.

6.1.1. Mantissas of regressive-precision vectors. Starting with the regressive-precision vectors $\hat{u}_{0:L}$, $\hat{r}_{0:L}$, and $\hat{y}_{0:L}$, assume that the number of DoFs on level ℓ is $n_\ell \approx c2^{d\ell}$, with a positive constant c possibly dependent of p . Recall that a regressive($+k, b$) precision vector comprises $k(L - \ell) + b$ bits on level ℓ . Multiplying by n_ℓ and summing over all grids, we find the total number of bits used:

$$(21) \quad N_d^{\hat{u}, \hat{r}, \hat{y}}(k, b) \approx c \sum_{\ell=0}^L (k(L - \ell) + b) 2^{d\ell} \stackrel{d \neq 0}{<} \left(\frac{2^d}{2^d - 1} b + \frac{2^d}{(2^d - 1)^2} k \right) n_L \in \mathcal{O}(n_L).$$

This establishes linear storage cost w.r.t. the number of unknowns. The constant $2^d(2^d - 1)^{-1}$ is 2 in 1D, $\frac{4}{3}$ in 2D, and $\frac{8}{7}$ in 3D, and is therefore small.

6.1.2. Mantissas of temporary vectors. The remaining vectors $\hat{z}_{0:L}$, $\hat{u}_{0:L}$, and $\hat{t}_{0:L}$ require progressive precision, but only $\delta(M)$ (cf. (19)) entries are stored in the optimized Algorithms 5 and 6. Here, M is the matrix that maximizes $\delta(M)$ among those applied to the respective temporary vector. Concretely, this is A for \hat{u} and \hat{z} and R for \hat{t} when using B-splines for the finite element discretization. Assuming the unknowns constitute a uniform grid and are ordered lexicographically, it has been established in section 5 that $\delta(M_\ell) \approx (w(M_\ell) - 1)n_\ell^{(d-1)/d} =: \tilde{c}_\ell n_\ell^{(d-1)/d}$.

Further assuming that the stencil width of the relevant matrices is independent of ℓ , the storage cost of \hat{u} and \hat{t} in Algorithm 6 and \hat{z} in Algorithm 5 are given by (22) and (23), respectively, where $a_L := kL + b$. In all cases, the space complexity is strictly less than $\mathcal{O}(n_L)$.

$$(22) \quad \hat{N}_d^{\hat{u}, \hat{t}}(a_L) = \sum_{\ell=0}^L a_L \delta(M_\ell) \approx \tilde{c} a_L \sum_{\ell=0}^L n_\ell^{\frac{d-1}{d}}$$

$$\leq \begin{cases} c^{\frac{d-1}{d}} \tilde{c} a_L (L + 1) \in \mathcal{O}(\log^2 n_L), & d = 1 \\ \frac{2^{d-1}}{2^{d-1}-1} \tilde{c} a_L n_L^{\frac{d-1}{d}} \in \mathcal{O}(n_L^{\frac{d-1}{d}} \log n_L), & d > 1 \end{cases}$$

$$(23) \quad \hat{N}_d^{\hat{z}}(k, b) = \sum_{\ell=0}^L (k\ell + b) \delta(M_\ell) \leq \sum_{\ell=0}^L a_L \delta(M_\ell) = \hat{N}_d^{\hat{u}, \hat{t}}(a_L)$$

6.1.3. Exponents. Apart from the mantissa, a floating point number also carries an exponent. The exponents of the compact solution vector decrease by $p + 1$ for each refinement level. Consequently, storing one exponent for each DoF would require $\mathcal{O}(n_L \log \log n_L)$ memory.

Therefore, we instead store \hat{u}_ℓ , \hat{r}_ℓ , and \hat{y}_ℓ for all $0 \leq \ell \leq L$ in block floating point (BFP) format [28], rendering the storage cost of exponents negligible. In BFP format, the vector is divided into few blocks. Each block comprises several mantissas, but only a single exponent scaling all mantissas. The extreme case, in which only a single exponent is stored for the entire vector, is also known as scaled fixed-point format. The applicability of BFP to mixed-precision multigrid methods has been demonstrated in [14].

One of the difficulties of this format is that the maximal exponent must be known before the mantissas can be normalized. In practice, the exponent might be known/estimated a priori [14]. Depending on how good the estimate is, the mantissa's size can be temporarily increased to allow for an inaccurate guess. This technique typically requires normalization after the computation, effectively doubling the memory traffic. If no (good) estimation is available, the values can be computed twice: once to determine the maximum exponent and a second time to store the values (according to the BFP exponent) [14].

Both re-normalization and re-computation can be avoided by increasing the number of blocks/exponents to b , with b being the number of bits in each mantissa. As the entries of the vector are computed, we keep track of the currently largest known exponent and normalize the current mantissa to that exponent. This exponent and associated mantissas constitute one block of the BFP vector. The next block starts when a larger exponent is encountered. Finally, to make the storage cost of the exponents independent of the vector size, note that storing only the b largest exponents suffices to recover all entries to single-exponent BFP accuracy: The other exponents are smaller by at least b compared to the largest exponent. Therefore, those entries would be truncated to zero in single-exponent BFP precision, irrespective of the actual value of the exponent or mantissa. Hence, at most b exponents and block-sizes must be stored to match the accuracy of the scaled fixed-point format.

To achieve linear space complexity, we use the BFP format for \hat{u}_ℓ , \hat{r}_ℓ , and \hat{y}_ℓ . Stencil entries and the temporary vectors \hat{z}_ℓ , \hat{u}_ℓ , and \hat{t}_ℓ have linear space complexity even in FP format because only few entries reside in memory at a time. Concretely, we found that the temporaries' exponents also grow linearly with L , and can therefore be stored with $\mathcal{O}(n_L^{(d-1)/d} \log \log n_L) \subsetneq \mathcal{O}(n_L)$ bits. To avoid overcomplicating matters, we use the usual FP format for stencils and temporaries. Therefore, whenever one of the arguments to an arithmetic operation is stored in FP format, the BFP argument is converted to its FP representation before performing the operation in FP arithmetic. In particular, all stencil applications use FP arithmetic and entail the associated rounding behavior. While we use BFP only where it is required for linear space complexity, storing and computing everything in BFP format as in [14] has the additional advantage of relying solely on integer arithmetic, which is cheaper than FP arithmetic.

6.1.4. Comparison to progressive precision FMG in BFP arithmetic.

To demonstrate that the improved asymptotics pay off at realistic problem sizes, we estimate the memory consumption of the isolated solution vector and an entire FMG implementation using the formulas from above. The baseline for the comparison is FMG in progressive precision BFP arithmetic (BFPMG) [14]. To the best of our knowledge, this is the current state-of-the-art in terms of memory efficiency. We make the following assumptions: BFPMG is implemented in a memory-efficient manner. In particular, the coarse-grid solution vector is freed immediately after computing the FMG prolongation. Moreover, during the V-cycle, memory is required only for the vectors \hat{u}_L , \hat{r}_L , \hat{r}_{L-1} , and $\hat{y}_{0:L}$. As in compact multigrid (CMG), matrices and RHS are assembled on-the-fly and do not consume memory. Lastly, we assume that no BFP normalizations are performed within the general matrix-vector product (gemv) routines and thus no additional storage is required in gemv operations nor the smoother. For both algorithms, we take the same precision increase and constants for solution vector, residual, and correction that we determine in section 7. The important difference is that BFPMG uses progressive instead of regressive precision.

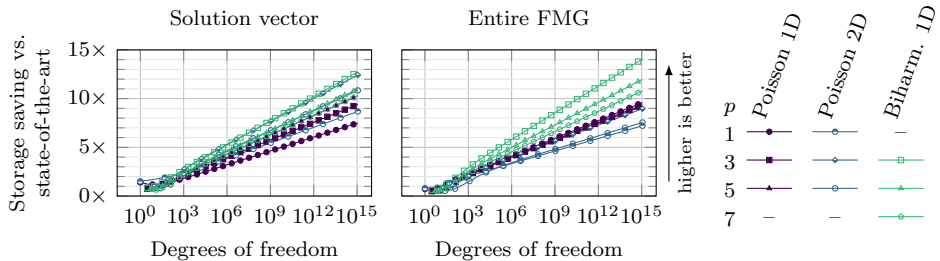


FIG. 4. *Estimated memory savings of compact multigrid compared to discretization-error accurate FMG in progressive BFP precision [14] (current state-of-the-art) for varying polynomial degrees. Here, we calculate with the experimentally determined constants from Table 2. A marker is placed every second refinement level.*

Figure 4 shows the estimated memory savings for the model problems discussed in section 7: Poisson’s equation in 1D and 2D ($m = 1$) and the biharmonic equation in 1D ($m = 2$). For problem sizes where even the memory capacity of an entire supercomputer becomes prohibitive [10], savings of around an order of magnitude are attainable. For BFPMG, the storage cost is primarily determined by the size of the precision increment, whereas for CMG, the (constant) bit-width of the finest grid is most important. Hence, the savings in the FMG solver increase with m , the precision increment of residual and correction. In contrast, no clear trend is visible w.r.t. the polynomial degree p , because with increasing p both the solution vector’s precision increment but also the number of bits on the finest grid increase (cf. Table 2).

6.2. Computation. The time complexity of our scheme is $\mathcal{O}(n_L)$ arithmetic operations. As in previous work [20, 26, 14], the arithmetic must be performed in progressively higher precision. Algorithms 5 and 6 contain the bulk of the overall work. Just as with a standard multigrid V-cycle, Algorithm 5 comprises one product with the system matrix, a smoothing step, and some grid transfers on each level. The residual computation, on the other hand, is more expensive than in a standard method because it requires prolongating all sections of the compact solution to the finest grid. Moreover, we directly restrict the residual to the entire grid hierarchy, adding one restriction per level to the overall work (which would normally be part of the V-cycle).

6.3. Communication. $\mathcal{O}(n_L \log n_L)$ bits are transferred between memory and compute unit, matching the already known progressive precision FMG [20, 26, 14]. The dominating term stems from the temporaries in Algorithms 5 and 6. While the loop transformation from section 5 reduces the storage complexity, it does not change the amount of communication. With or without optimization, all entries of the temporaries are written/read to/from memory. On the finest grid, this amounts to n_L elements with $\mathcal{O}(\log n_L)$ bits each. However, another benefit of the optimizations is that they increase spatial and temporal locality of memory accesses. Potentially, this makes these accesses less expensive, e.g., on CPUs if the optimized temporaries fit entirely into cache.

7. Numerical experiments. In this section, numerical results demonstrate that the proposed compact FMG solver achieves discretization-error accuracy with linear storage complexity and a linear number of operations. Our implementation builds on the GMP [11] and MPFR [9] libraries for arbitrary precision arithmetic,

and the G+SMO library [19] for the FEM discretization.

7.1. Setup. We consider the homogeneous Dirichlet problem for Poisson's equation in one and two dimensions and the biharmonic equation in one dimension. Specifically, we define $\Omega = (0, 1)$ and $f(x) \in L^2(\Omega^d)$, and seek to approximate $u(x) \in C^{2m}$ so that

$$(24) \quad \begin{aligned} -\Delta u(x) &= f(x) && \text{in } \Omega^d, \\ u(x) &= 0 && \text{on } \partial(\Omega^d), \end{aligned} \quad (25) \quad \begin{aligned} u''''(x) &= f(x) && \text{in } \Omega, \\ u(x) &= u'(x) = 0 && \text{on } \partial\Omega, \end{aligned}$$

where $d \in \{1, 2\}$, $m = 1$ in (24), and $d = 1$, $m = 2$ in (25).

To allow assessment of the error, we manufacture the analytical solutions $u(x) = x(1-x)\cos(\frac{\pi}{2}x)$ for $(m, d) = (1, 1)$ (Poisson's equation (24), 1D), $u(x_0, x_1) = x_0(1-x_0)\cos(\frac{\pi}{2}x_0)x_1(1-x_1)\cos(\frac{\pi}{2}x_1)$ for $(m, d) = (1, 2)$ (Poisson's equation (24), 2D), and $u(x) = 1 - \cos(2\pi x)$ for $(m, d) = (2, 1)$ (biharmonic equation (25), 1D). The model problems are discretized using B-spline finite elements of polynomial degree p ($p = 1, \dots, 5$ for Poisson's equation, $p = 3, \dots, 7$ for the biharmonic equation). As described in section 4, we fix the number of compact V-cycles ν to $\nu = 1$ and only vary the number of IR iterations N per level in the FMG solver.

To verify our implementation, we compute a reference solution u_L using a standard FMG solver in FP arithmetic with 200 $((m, d) = (1, 1))$, 100 $((m, d) = (1, 2))$, and 250 $((m, d) = (2, 1))$ bits mantissas and using 30 V(2, 1)-cycles per level to achieve discretization error. The compact FMG algorithm is considered successful if the error of its computed approximation \tilde{u}_L is within twice the discretization error, i.e.,

$$(26) \quad \|\tilde{u}_L - u\|_{H^m} \leq 2\|u_L - u\|_{H^m},$$

and the convergence order is at most 0.05 below the theoretically optimal rate, i.e.,

$$(27) \quad -\log_2 \left(\frac{\|\tilde{u}_L - u\|_{H^m}}{\|\tilde{u}_{L-1} - u\|_{H^m}} \right) \geq (p - m + 1) - 0.05,$$

for all levels $L \geq 4$, ignoring the preasymptotic region.

We perform a simple experimental optimization to determine the remaining parameters N (number of IR iterations per level) and b_1, b_2, b_3, b_4 (the precision constants in Table 1) of the compact FMG algorithm. Initially, we fix $b_1 = b_3 = b_4 = 30$, $N = 12$ (which is more than sufficient to recover the convergence criteria (26) and (27)) and increase b_2 (starting from $b_2 = 1$) until (26) and (27) hold for $L_{\max} = 8$ ($d = 1$) and $L_{\max} = 5$ ($d = 2$). This is done for each problem and for each polynomial degree p individually. Once the criteria are satisfied, we add an additional bit to b_2 (to add some stability when going to finer grids later) and ensure that the convergence criteria are still met. We then fix b_2 and proceed to tune b_1, b_4, b_3 , and lastly N (starting from $N = 1$) in the same way (also adding one additional bit and IR iteration respectively). It is certainly possible that the constants depend on each other, and that a different ordering of this search procedure would lead to different results. We chose this specific ordering hoping to find the smallest possible b_2 as that is likely to be the one constant that has the most impact on the storage savings. However, we do not claim that this is an optimal way to choose the parameters. In any case, having optimized the constants for these coarse problems, we fix all the precisions and run the experiments up to levels $L_{\max} = 22$ ($d = 1$) and $L_{\max} = 11$ ($d = 2$).

7.2. Results. The computed constants are listed in Table 2. Most are eight bits or lower, with exceptions occurring only for $p \geq 5$. The compact vectors may use as

TABLE 2

Number of IR iterations N per FMG level (cf. [Algorithm 3](#)) and precision constants b_1, b_2, b_3, b_4 (cf. [Table 1](#)) used in the experiments. The sign-bit is included in the numbers listed here. Note that for the regressive cases, the constants b_1 and b_2 are exactly the number of bits on the finest FMG level L_{\max} , independent of h .

| p | | 1 | 2 | 3 | 4 | 5 | 6 | 7 |
|---|------------|---|---|---|---|----|----|----|
| N (IR iterations per FMG level) | Poisson 1D | 4 | 3 | 4 | 5 | 9 | – | – |
| | Poisson 2D | 3 | 2 | 4 | 7 | 9 | – | – |
| | Biharm. 1D | – | – | 6 | 4 | 5 | 5 | 11 |
| b_1 (regressive(+ $p+1, b_1$) ▲) (\hat{u}) | Poisson 1D | 5 | 5 | 7 | 8 | 9 | – | – |
| | Poisson 2D | 4 | 5 | 5 | 7 | 9 | – | – |
| | Biharm. 1D | – | – | 4 | 6 | 8 | 11 | 12 |
| b_2 (regressive(+ m, b_2) △) (\hat{r}, \hat{y}) | Poisson 1D | 3 | 4 | 4 | 4 | 5 | – | – |
| | Poisson 2D | 4 | 4 | 4 | 5 | 6 | – | – |
| | Biharm. 1D | – | – | 4 | 4 | 5 | 5 | 6 |
| b_3 (progressive(+ $p+m+1, b_3$) ▼) (matrices, \hat{f} in FMGRESIDUAL) | Poisson 1D | 2 | 4 | 6 | 7 | 11 | – | – |
| | Poisson 2D | 2 | 3 | 4 | 7 | 15 | – | – |
| | Biharm. 1D | – | – | 2 | 2 | 2 | 3 | 3 |
| b_4 (progressive(+ m, b_4) ▽) (matrices, \hat{z} in CFAS) | Poisson 1D | 2 | 2 | 2 | 2 | 4 | – | – |
| | Poisson 2D | 2 | 2 | 2 | 2 | 2 | – | – |
| | Biharm. 1D | – | – | 3 | 2 | 2 | 2 | 2 |

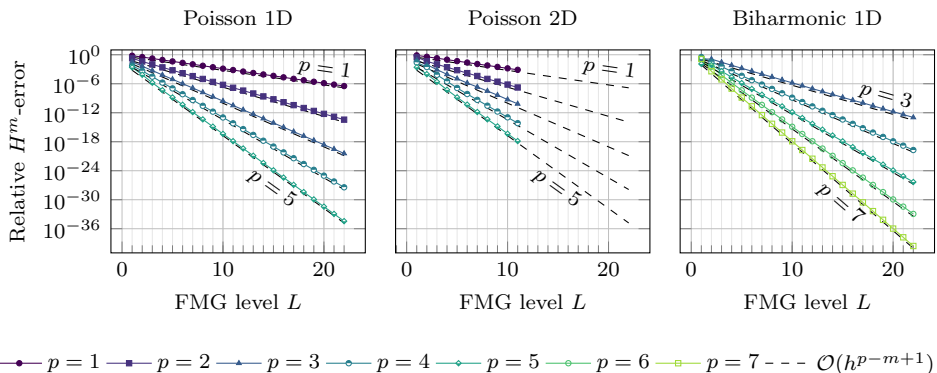


FIG. 5. Relative H^m -error $\|\tilde{u}_L - u\|_{H^m} / \|u\|_{H^m}$ of the computed compact solution \tilde{u}_L to Poisson's equation (24) ($m = 1, d \in \{1, 2\}$) and the biharmonic equation (25) ($m = 2, d = 1$) discretized with B-splines of degree p (using parameters from [Table 2](#)). The numerical results show the expected convergence rate $\mathcal{O}(h^{p-m+1})$ consistent with theoretical results, where $h = 2^{-L}$. It is worth comparing these results to [Figure 1](#) to get an idea of the limits of common IEEE floating-point formats.

few as three bits for the finest section, one of which represents the sign. Moreover, the number of IR iterations is welcomely low, considering that only one Gauss-Seidel sweep per level is performed in each iteration. Generally, we observe some dependence on the equation and polynomial degree p . This is especially true for N, b_1 , and b_3 . This is expected because the lower discretization error inherent to higher-order methods must be balanced by lower quantization error. We observe that b_2 and b_4 depend only mildly on d, m , and p .

[Figure 5](#) shows the relative H^m -error, $\|\tilde{u}_L - u\|_{H^m} / \|u\|_{H^m}$ of the computed com-

pact solution \tilde{u}_L against the analytically known solution u . As can be seen, our algorithm achieves the asymptotically optimal convergence rate $\mathcal{O}(h^{p-m+1})$, which is limited by the discretization error. As expected, the convergence curves for Poisson’s equation are essentially identical in 1D and 2D. Notably, using linear elements for the 1D Poisson equation, as few as 5 bits for $\hat{u}_{L_{\max}}$ and 3 bits each for $\hat{r}_{L_{\max}}$ and $\hat{y}_{L_{\max}}$ are required per DoF. This means that for all vectors combined, only 11 bits per fine-grid point, about one sixth of a double-precision vector, must be stored to achieve discretization error for any h . We highlight that using seventh-order elements, we computed a discretization-error-accurate solution to the biharmonic equation with an H^2 -error of less than 10^{-39} in as few as 12 bits for the solution vector on the finest grid. It is worth comparing these results to Figure 1 to get an idea of the limits of common IEEE floating-point formats.

8. Conclusion. In this work, we have reduced the space complexity of discretization-error accurate multigrid from $\mathcal{O}(n \log n)$ to $\mathcal{O}(n)$. It is estimated that for state-of-the-art problems limited by memory capacity [10], this corresponds to a memory footprint reduction of about an order of magnitude. The time complexity is the same as that of well-known multigrid methods in standard arithmetic.

While a theoretical framework remains to be worked out, we have found that, in many cases, six bits or fewer provide sufficient precision to store the solution, residual, and correction on the finest grid. Contemporary hardware may not provide support for the exact bit widths we require, so in practice the data must be packed bit-wise into memory and converted to a supported data-type on load. Because the memory bandwidth of modern hardware lags behind the computational performance, the cost of this conversion is generally insignificant compared to the communication cost [13]. The coarsest grid, by contrast, may require bit-widths beyond the widest data-type implemented in hardware. The needed high-precision arithmetic can be efficiently emulated using low-precision integer arithmetic [21].

A parallel implementation of our algorithms is out of scope of this article, but we presently do not see any reason why a parallel implementation with up to $\mathcal{O}(n/\log n)$ processes would not achieve linear memory complexity. Especially in the parallel setting, polyhedral compilers [8, 3] could prove valuable for implementing the presented memory optimizations.

REFERENCES

- [1] M. AINSWORTH, O. TUGLUK, B. WHITNEY, AND S. KLASKY, *Multilevel techniques for compression and reduction of scientific data—the univariate case*, *Comput. Visual Sci.*, 19 (2018), pp. 65–76, <https://doi.org/10.1007/s00791-018-00303-9>.
- [2] A. H. BAKER, R. D. FALGOUT, T. V. KOLEV, AND U. M. YANG, *Multigrid smoothers for ultraparallel computing*, *SIAM J. Sci. Comput.*, 33 (2011), pp. 2864–2887, <https://doi.org/10.1137/100798806>.
- [3] U. BONDHUGULA, A. HARTONO, J. RAMANUJAM, AND P. SADAYAPPAN, *A practical automatic polyhedral parallelizer and locality optimizer*, in *Proceedings of the 29th ACM SIGPLAN Conference on Programming Language Design and Implementation*, Association for Computing Machinery, 2008, pp. 101–113, <https://doi.org/10.1145/1375581.1375595>.
- [4] J. H. BRAMBLE, J. E. PASCIAK, AND J. XU, *Parallel multilevel preconditioners*, *Math. Comp.*, 55 (1990), pp. 1–22, <https://doi.org/10.1090/S0025-5718-1990-1023042-6>.
- [5] A. BRANDT AND O. E. LIVNE, *Multigrid techniques: 1984 guide with applications to fluid dynamics*, SIAM, Philadelphia, revised ed., 2011, <https://doi.org/10.1137/1.9781611970753>.
- [6] W. L. BRIGGS, V. E. HENSON, AND S. F. MCCORMICK, *A Multigrid Tutorial*, SIAM, Philadelphia, 2nd ed., 2000, <https://doi.org/10.1137/1.9780898719505>.
- [7] R. D. FALGOUT AND P. S. VASSILEVSKI, *On generalizing the algebraic multigrid framework*, *SIAM J. Numer. Anal.*, 42 (2004), pp. 1669–1693, <https://doi.org/10.1137/>

- S0036142903429742.
- [8] P. FEAUTRIER AND C. LENGAUER, *Polyhedron model*, in Encyclopedia of Parallel Computing, D. Padua, ed., Springer, Boston, 2011, pp. 1581–1592, https://doi.org/10.1007/978-0-387-09766-4_502.
 - [9] L. FOUSSE, G. HANROT, V. LEFÈVRE, P. PÉLISSIER, AND P. ZIMMERMANN, *MPFR: A multiple-precision binary floating-point library with correct rounding*, ACM Trans. Math. Software, 33 (2007), 13, <https://doi.org/10.1145/1236463.1236468>.
 - [10] B. GMEINER, M. HUBER, L. JOHN, U. RÜDE, AND B. WOHLMUTH, *A quantitative performance study for Stokes solvers at the extreme scale*, Journal of Computational Science, 17 (2016), pp. 509–521, <https://doi.org/10.1016/j.joocs.2016.06.006>.
 - [11] T. GRANLUND ET AL., *GMP: The GNU multiple precision arithmetic library*, 2020, <https://gmplib.org/>. Version 6.2.1.
 - [12] M. GRIEBEL, *Multilevel algorithms considered as iterative methods on semidefinite systems*, SIAM J. Sci. Comput., 15 (1994), pp. 547–565, <https://doi.org/10.1137/0915036>.
 - [13] T. GRÜTZMACHER, H. ANZT, AND E. S. QUINTANA-ORTÍ, *Using Ginkgo’s memory accessor for improving the accuracy of memory-bound low precision BLAS*, Softw Pract Exper., 53 (2023), pp. 81–98, <https://doi.org/10.1002/spe.3041>.
 - [14] N. KOHL, S. F. MCCORMICK, AND R. TAMSTORF, *Multigrid methods using block floating point arithmetic*, SIAM J. Sci. Comput., 46 (2024), pp. S202–S224, <https://doi.org/10.1137/23M1581819>.
 - [15] D. KOLOMENSKIY, R. ONISHI, AND H. UEHARA, *WaveRange: wavelet-based data compression for three-dimensional numerical simulations on regular grids*, J Vis, 25 (2022), pp. 543–573, <https://doi.org/10.1007/s12650-021-00813-8>.
 - [16] M. KRONBICHLER AND W. A. WALL, *A performance comparison of continuous and discontinuous Galerkin methods with fast multigrid solvers*, SIAM J. Sci. Comput., 40 (2018), pp. A3423–A3448, <https://doi.org/10.1137/16M110455X>.
 - [17] S. LI, N. MARSAGLIA, C. GARTH, J. WOODRING, J. CLYNE, AND H. CHILDS, *Data reduction techniques for simulation, visualization and data analysis*, Computer Graphics Forum, 37 (2018), pp. 422–447, <https://doi.org/10.1111/cgf.13336>.
 - [18] X. LIANG, B. WHITNEY, J. CHEN, L. WAN, Q. LIU, D. TAO, J. KRESS, D. PUGMIRE, M. WOLF, N. PODHORSKI, AND S. KLASKY, *MGARD+: Optimizing multilevel methods for error-bounded scientific data reduction*, IEEE Transactions on Computers, 71 (2022), pp. 1522–1536, <https://doi.org/10.1109/TC.2021.3092201>.
 - [19] A. MANTZAFLARIS, *An overview of geometry plus simulation modules*, in Mathematical Aspects of Computer and Information Sciences, D. Slamanig, E. Tsigaridas, and Z. Zafeirakopoulos, eds., Springer, Cham, 2020, pp. 453–456, https://doi.org/10.1007/978-3-030-43120-4_35.
 - [20] S. F. MCCORMICK, J. BENZAKEN, AND R. TAMSTORF, *Algebraic error analysis for mixed-precision multigrid solvers*, SIAM J. Sci. Comput., 43 (2021), pp. S392–S419, <https://doi.org/10.1137/20M1348571>.
 - [21] H. OOTOMO, K. OZAKI, AND R. YOKOTA, *DGEMM on integer matrix multiplication unit*, The International Journal of High Performance Computing Applications, 38 (2024), pp. 297–313, <https://doi.org/10.1177/10943420241239588>.
 - [22] V. PAN AND J. REIF, *Compact multigrid*, SIAM J. Sci. Stat. Comput., 13 (1992), pp. 119–127, <https://doi.org/10.1137/0913007>.
 - [23] V. RESHNAK, E. FERGUSON, Q. GONG, N. VIDAL, R. ARCHIBALD, AND S. KLASKY, *Lifting MGARD: Construction of (pre)wavelets on the interval using polynomial predictors of arbitrary order*, Applied Mathematics for Modern Challenges, 2 (2024), pp. 409–432, <https://doi.org/10.3934/ammc.2024021>.
 - [24] E. J. STOLLNITZ, T. D. DEROSE, AND D. H. SALESIN, *Wavelets for computer graphics: Theory and applications*, Morgan Kaufmann Publishers, San Francisco, 1996.
 - [25] G. STRANG AND G. J. FIX, *An analysis of the finite element method*, Wellesley-Cambridge Press, Wellesley, 2nd ed., 2008.
 - [26] R. TAMSTORF, J. BENZAKEN, AND S. F. MCCORMICK, *Discretization-error-accurate mixed-precision multigrid solvers*, SIAM J. Sci. Comput., 43 (2021), pp. S420–S447, <https://doi.org/10.1137/20M1349230>.
 - [27] V. THURNER, *Eine ganzzahlige Arithmetik zur adaptiven Lösung der Poisson-Gleichung mit hierarchischen Basen*, diploma thesis, Technische Universität München, 1994.
 - [28] J. H. WILKINSON, *Rounding Errors in Algebraic Processes*, SIAM, Philadelphia, 2023, <https://doi.org/10.1137/1.9781611977523>.

SUPPLEMENTARY MATERIALS: MULTIGRID WITH LINEAR STORAGE COMPLEXITY *

DANIEL BAUER [†], NILS KOHL [‡], STEPHEN F. MCCORMICK[§], AND RASMUS TAMSTORF [¶]

SM1. Review of multigrid. This section gives a brief introduction into existing multigrid theory. It familiarizes the reader with the multigrid variant that our compact algorithm is based on, which is a full multigrid (FMG) method using iterative refinement (IR) [SM5] and the full approximation scheme (FAS) to solve the residual equation on each level. For details, the reader is referred to [SM2, SM3].

SM1.1. Multigrid V-cycle. The multigrid V-cycle is an iterative solver for elliptic partial differential equations (PDEs) with h -independent convergence. In other words, the solution can be computed to a *fixed* target accuracy with a number of V-cycles independent of the grid spacing. This sets it apart from stationary iterations and Krylov methods, whose performance typically degrades as h decreases. There are two different formulations of multigrid: the correction scheme (CS) and FAS. For linear systems, CS and FAS are equivalent.

SM1.1.1. Correction scheme. As outlined in section 2, we are solving an elliptic PDE by discretizing it on a set of $L + 1$ nested grids. Prolongation matrices $P_\ell \in \mathbb{R}^{n_\ell \times n_{\ell-1}}$ transfer vectors from level $\ell - 1$ to level ℓ . In this section, we write the discretized PDE on refinement level L as

$$(SM1) \quad A_L \hat{y}_L = \hat{r}_L.$$

In the following, we refer to the exact solution of (SM1) as $A_L^{-1} \hat{r}_L$ and an approximate computed iterate as \hat{y}_L , avoiding the need of iteration indices. For example, the error is written as $\hat{e}_L = A_L^{-1} \hat{r}_L - \hat{y}_L$.

This error consists of smooth and oscillatory components. Key to the algorithm's efficiency is using two different methods to target these two errors individually. Both must be effective at reducing their respective part of the spectrum but typically perform poorly as a standalone solver.

Reducing oscillatory error modes is the responsibility of the *smoother*. Typical choices are relaxation methods of the form [SM4]

$$(SM2) \quad \hat{y}_L \leftarrow \hat{y}_L + M_L(\hat{r}_L - A_L \hat{y}_L),$$

*The author/s would like to thank the NHR-Verein e.V. (www.nhr-verein.de) for supporting this work/project within the NHR Graduate School of National High Performance Computing (NHR). The authors gratefully acknowledge support through the joint project CoMPS (<https://gauss-allianz.de/en/project/title/CoMPS>) (grant 16ME0647K) funded by the German Federal Ministry of Research, Technology and Space. The authors gratefully acknowledge the Gauss Centre for Supercomputing e.V. (<https://www.gauss-centre.eu>) for funding this project by providing computing time on the GCS Supercomputer SuperMUC-NG and friendly user access during the pilot operation of the GCS Supercomputer SuperMUC-NG Phase 2 at Leibniz Supercomputing Centre (<https://www.lrz.de>).

[†]Friedrich-Alexander-Universität Erlangen-Nürnberg (FAU), Erlangen National High Performance Computing Center (NHR@FAU), (daniel.j.bauer@fau.de).

[‡]Dept. of Earth and Environmental Sciences, Ludwig-Maximilians-Universität München (LMU).

[§]University of Colorado at Boulder, Boulder, CO.

[¶]Independent researcher.

where M_L approximates A_L^{-1} . Examples include weighted Jacobi, Gauss-Seidel, and polynomial smoothers [SM1].

After a few iterations of the smoother, the error is typically dominated by smooth components. Assuming that the remaining smooth error can be represented reasonably well on a coarser grid ($\hat{e}_L \approx P_L \hat{d}_{L-1}$), it can be well approximated by solving the residual equation $A_L \hat{e}_L = \hat{r}_L - A_L \hat{y}_L$ restricted to the next coarser grid:

$$(SM3) \quad \underbrace{R_L A_L P_L}_{A_{L-1}} \hat{d}_{L-1} = R_L (\hat{r}_L - A_L \hat{y}_L).$$

Here, the restriction $R_\ell \in \mathbb{R}^{n_{\ell-1} \times n_\ell}$, $1 \leq \ell \leq L$, transfers vectors from one grid to the next coarser grid and is typically defined as $R_\ell := P_\ell^T$.

Because (SM3) is formulated on a coarser grid, it can typically be solved efficiently. To that end, note first that, it has essentially the same structure as the fine-grid problem (SM1) and, second, that smooth modes from the fine grid appear more oscillatory w.r.t. the coarse grid. Therefore, (SM3) is best solved recursively, by applying a smoother and computing a correction from a yet coarser grid. The recursion is stopped once the system is small enough to be solved directly by a *coarse-grid solver*.

Once the correction \hat{d}_{L-1} is computed, it is prolonged and added to the solution:

$$(SM4) \quad \hat{y}_L \leftarrow \hat{y}_L + P_L \hat{d}_{L-1}.$$

This reduces the smooth error components that contaminate \hat{y}_L . It is common to apply additional post-smoothing steps after updating the solution. Generally, both the smoother and the coarse-grid solver are approximate. Moreover, the error left after smoothing is typically not perfectly in the range of P , meaning that the correction typically introduces new albeit fairly small additional oscillatory errors. Therefore, more V-cycles are usually required to attain satisfactory accuracy, with increasingly more as the grid becomes increasingly finer.

SM1.1.2. Full approximation scheme. FAS is most commonly used to solve nonlinear problems. Nevertheless, it has applications in linear problems as well. For example, one byproduct is an error estimator, which can be used for stopping criteria and adaptive grid refinement [SM2]. Moreover, it leads to τ -extrapolation, which raises the approximation order without using higher-order elements [SM2]. For our purposes, the most important property of FAS is that it gives accurate solutions to the fine grid equation, but on the coarse grids.

FAS performs the same steps as CS, but with a different coarse-grid variable. Here, the coarse-grid variable is not the correction, but instead closely approximates the solution to the fine-grid equation. It is defined as

$$(SM5) \quad \hat{y}_{L-1} := \tilde{R}_L \hat{y}_L + \hat{d}_{L-1},$$

where \tilde{R} is a restriction operator defined on the primal space (unlike R which is defined on the dual space), and \hat{d}_{L-1} is the same coarse correction as in (SM3). One typically has some freedom in choosing \tilde{R} without sacrificing efficiency [SM2]. We comment on our choice in subsection 3.2. \hat{y}_{L-1} is found by (approximately) solving the FAS coarse-grid equation

$$(SM6) \quad \begin{aligned} A_{L-1} \hat{y}_{L-1} &= A_{L-1} \tilde{R}_L \hat{y}_L + R_L (\hat{r}_L - A_L \hat{y}_L) \\ &= R_L \hat{r}_L + \underbrace{(A_{L-1} \tilde{R}_L \hat{y}_L - R_L A_L \hat{y}_L)}_{\hat{\tau}_L}. \end{aligned}$$

Algorithm SM1 Full multigrid iterating on the original equation on each level.

| | | | |
|--|---|---|-----------------------------|
| | \mathcal{L} | continuous linear operator | |
| | $f(x)$ | continuous RHS | |
| <i>Input.</i> | L_{\max} | index of finest grid | |
| | N | number of IR-iterations | |
| | ν | number of V-cycles per FMG level | |
| <i>Output.</i> Solution $\hat{u}_{L_{\max}}$. | | | |
| 1 | $(A_0, \hat{f}_0) \leftarrow \text{DISCRETIZE}(\mathcal{L}, f(x), L = 0)$ | | |
| 2 | $\hat{u}_0 \leftarrow A_0^{-1} \hat{f}_0$ | | |
| 3 | for $L = 1 \dots L_{\max}$ step 1 | | |
| 4 | 1 | $(A_{0:L}, P_{1:L}, R_{1:L}, \hat{f}_L) \leftarrow \text{DISCRETIZE}(\mathcal{L}, f(x), L)$ | |
| 5 | 2 | $\hat{u}_L \leftarrow P_L \hat{u}_{L-1}$ | |
| 6 | repeat ν times | | |
| 7 | 1 | $\hat{u}_L \leftarrow \text{V-CYCLE}(A, P, R, \hat{u}_L, \hat{f}_L)$ | \triangleright CS or FAS. |
| 8 | return $\hat{u}_{L_{\max}}$ | | |

This equation is found by replacing \hat{d}_{L-1} in (SM3) with the expression given by (SM5) and rearranging. $\hat{\tau}_L$ is known as the *fine-to-coarse defect correction*, which modifies the coarse-grid equation so that at convergence its solution coincides with the (restricted) fine-grid solution $\tilde{R}_L A_L^{-1} \hat{r}_L$.

Having found a good approximation on the coarse grid (again through recursion), the fine-grid variable is updated according to

$$(SM7) \quad \hat{y}_L \leftarrow \hat{y}_L + P_L \hat{d}_{L-1} = \hat{y}_L + P_L (\hat{y}_{L-1} - \tilde{R}_L \hat{y}_L).$$

SM1.2. Full multigrid. As h reduces, so does the discretization error. While V-cycles reduce the error by a fixed amount in linear time, achieving discretization error takes an increasing number of cycles. That is why either CS or FAS is often best used in an FMG scheme, as we now explain.

FMG solves the PDE on successively finer grids with an accuracy comparable to the respective discretization error. To avoid confusing the variables of the outer FMG solver and the inner V-cycle, we now consider the PDE $\mathcal{L}u(x) = f(x)$.

SM1.2.1. Iterating on the original equation on each FMG level. In its classical form, as given in Algorithm SM1, the solution from the previous FMG level $P_L \hat{u}_{L-1}$ is used as initial guess for the next finer grid. Because this initial guess is close to discretization error on the previous grid, the error contained within must only be reduced by a fixed factor to reduce it to discretization error on grid L . When measuring error in the energy norm, this factor is 2^{p-m+1} , where p is the polynomial degree of the discretization and $2m$ is the order of the PDE [SM7]. Due to the h -independent convergence of multigrid, a fixed number of V-cycles achieves this error reduction. This makes FMG optimal in the sense that it is discretization-error accurate and its arithmetic cost is equivalent to just a few relaxation sweeps, meaning that it has linear time complexity in infinite precision.

SM1.2.2. Using IR on each FMG level. A different formulation of FMG is laid out in Algorithm SM2. Instead of iterating on the original equation, it solves the residual/correction equation

$$(SM8) \quad A_L \hat{y}_L = \hat{r}_L := \hat{f}_L - A_L P_L \hat{u}_{L-1}$$

on each FMG level, and then adds the correction to the solution. A long-established technique known as IR is to compute the residual in higher precision, solve for the correction, and update the solution in a loop with $N \geq 1$ iterations [SM5, SM6].

Algorithm SM2 Full multigrid using iterative refinement on each level.

| | | |
|--|---|-----------------------------|
| \mathcal{L} | continuous linear operator | |
| $f(x)$ | continuous RHS | |
| <i>Input.</i> L_{\max} | index of finest grid | |
| N | number of IR-iterations | |
| ν | number of V-cycles per FMG level | |
| <i>Output.</i> Solution $\hat{u}_{L_{\max}}$. | | |
| 1 | $(A_0, \hat{f}_0) \leftarrow \text{DISCRETIZE}(\mathcal{L}, f(x), L = 0)$ | |
| 2 | $\hat{u}_0 \leftarrow A_0^{-1} \hat{f}_0$ | |
| 3 | for $L = 1 \dots L_{\max}$ step 1 | |
| 4 | $(A_{0:L}, P_{1:L}, R_{1:L}, \hat{f}_L) \leftarrow \text{DISCRETIZE}(\mathcal{L}, f(x), L)$ | |
| 5 | $\hat{u}_L \leftarrow P_L \hat{u}_{L-1}$ | |
| 6 | repeat N times | |
| 7 | $\hat{r}_L \leftarrow \hat{f}_L - A_L \hat{u}_L$ | |
| 8 | $\hat{y}_L \leftarrow 0$ | |
| 9 | repeat ν times | |
| 10 | $\hat{y}_L \leftarrow \text{V-CYCLE}(A, P, R, \hat{y}_L, \hat{r}_L)$ | \triangleright CS or FAS. |
| 11 | $\hat{u}_L \leftarrow \hat{u}_L + \hat{y}_L$ | |
| 12 | return $\hat{u}_{L_{\max}}$ | |

While equivalent to [Algorithm SM1](#) in infinite precision (if the total number of V-cycles is the same), this formulation facilitates reduced-precision arithmetic. Only the residual must be computed in relatively high precision, whereas the precision requirements on the V-cycle reduce significantly [[SM6](#), [SM8](#)]. Concretely, in contrast to \hat{u}_L requiring progressive precision with $p + 1$ bits increment, it is shown for $\nu = 1$ that the V-cycle can be performed with just m bits increment [[SM8](#)].

REFERENCES

- [SM1] A. H. BAKER, R. D. FALGOUT, T. V. KOLEV, AND U. M. YANG, *Multigrid smoothers for ultraparallel computing*, SIAM J. Sci. Comput., 33 (2011), pp. 2864–2887, <https://doi.org/10.1137/100798806>.
- [SM2] A. BRANDT AND O. E. LIVNE, *Multigrid techniques: 1984 guide with applications to fluid dynamics*, SIAM, Philadelphia, revised ed., 2011, <https://doi.org/10.1137/1.9781611970753>.
- [SM3] W. L. BRIGGS, V. E. HENSON, AND S. F. MCCORMICK, *A Multigrid Tutorial*, SIAM, Philadelphia, 2nd ed., 2000, <https://doi.org/10.1137/1.9780898719505>.
- [SM4] R. D. FALGOUT AND P. S. VASSILEVSKI, *On generalizing the algebraic multigrid framework*, SIAM J. Numer. Anal., 42 (2004), pp. 1669–1693, <https://doi.org/10.1137/S0036142903429742>.
- [SM5] N. J. HIGHAM, *Accuracy and stability of numerical algorithms*, no. 80, Society for Industrial and Applied Mathematics (SIAM, 3600 Market Street, Floor 6, Philadelphia, PA 19104), 2nd ed ed., 2002, <https://doi.org/10.1137/1.9780898718027>.
- [SM6] S. F. MCCORMICK, J. BENZAKEN, AND R. TAMSTORF, *Algebraic error analysis for mixed-precision multigrid solvers*, SIAM J. Sci. Comput., 43 (2021), pp. S392–S419, <https://doi.org/10.1137/20M1348571>.
- [SM7] G. STRANG AND G. J. FIX, *An analysis of the finite element method*, Wellesley-Cambridge Press, Wellesley, 2nd ed., 2008.
- [SM8] R. TAMSTORF, J. BENZAKEN, AND S. F. MCCORMICK, *Discretization-error-accurate mixed-precision multigrid solvers*, SIAM J. Sci. Comput., 43 (2021), pp. S420–S447, <https://doi.org/10.1137/20M1349230>.